

1 Adult dentate gyrus neurogenesis: a functional 2 model

3 Olivia Gozel^{1,2,*} and Wulfram Gerstner¹

4 ¹Laboratory of Computational Neuroscience, School of Life Sciences and School of
5 Computer and Communication Sciences, Brain-Mind Institute, Ecole Polytechnique
6 Fédérale de Lausanne, Lausanne, Switzerland

7 ²Current affiliation: Department of Neurobiology, University of Chicago, Chicago, IL
8 60637, USA

9 *gozel@uchicago.edu

10 Summary

11 In adult dentate gyrus neurogenesis, the link between maturation of newborn
12 neurons and their function, such as behavioral pattern separation, has remained
13 puzzling. By analyzing a theoretical model, we show that the switch from excita-
14 tion to inhibition of the GABAergic input onto maturing newborn cells is crucial
15 for their proper functional integration. When the GABAergic input is excitatory,
16 cooperativity drives the growth of synapses such that newborn cells become sen-
17 sitive to stimuli similar to those that activate mature cells. When GABAergic
18 input switches to inhibitory, competition pushes the configuration of synapses
19 onto newborn cells towards stimuli that are different from previously stored ones.
20 This enables the maturing newborn cells to code for concepts that are novel, yet
21 similar to familiar ones. Our theory of newborn cell maturation explains both
22 how adult-born dentate granule cells integrate into the preexisting network and
23 why they promote separation of similar but not distinct patterns.

24 Introduction

25 In the adult mammalian brain, neurogenesis, the production of new neurons,
26 is restricted to a few brain areas, such as the olfactory bulb and the dentate
27 gyrus (Deng et al., 2010). The dentate gyrus is a major entry point of input from
28 cortex, primarily entorhinal cortex (EC), to the hippocampus (Amaral et al.,

29 2007), which is believed to be a substrate of learning and memory (Jarrard,
30 1993). Adult-born cells in dentate gyrus mostly develop into dentate granule
31 cells (DGCs), the main excitatory cells that project to area CA3 of hippocam-
32 pus (Deng et al., 2010).

33 The properties of rodent adult-born DGCs change as a function of their mat-
34 uration stage, until they become indistinguishable from other mature DGCs at
35 approximately 8 weeks (Deng et al., 2010; Johnston et al., 2016) (Fig. 1a). Many
36 of them die before they fully mature (Dayer et al., 2003). Their survival is
37 experience-dependent, and relies upon NMDA receptor activation (Tashiro et al.,
38 2006). Initially, newborn DGCs have enhanced excitability (Schmidt-Hieber et al.,
39 2004; Li et al., 2017) and stronger synaptic plasticity than mature DGCs, reflected
40 by a larger LTP amplitude and a lower threshold for induction of LTP (Wang
41 et al., 2000; Schmidt-Hieber et al., 2004; Ge et al., 2007). Furthermore, after 4
42 weeks of maturation adult-born DGCs have only weak connections to interneu-
43 rons, while at 7 weeks of age their activity causes indirect inhibition of mature
44 DGCs (Temprana et al., 2015).

45 Newborn DGCs receive no direct connections from mature DGCs (Deshpande
46 et al., 2013; Alvarez et al., 2016) (yet see (Vivar et al., 2012)), but are indirectly ac-
47 tivated via interneurons (Alvarez et al., 2016; Heigele et al., 2016). At about three
48 weeks after birth, the γ -aminobutyric acid (GABAergic) input from interneurons
49 to adult-born DGCs switches from excitatory in the early phase to inhibitory in
50 the late phase of maturation (Ge et al., 2006; Deng et al., 2010) ('GABA-switch',
51 Fig. 1a). Analogous to a similar transition during embryonic and early postnatal
52 stages (Wang and Kriegstein, 2010), the GABA-switch is caused by a change in
53 the expression profile of chloride cotransporters. In the early phase of matura-
54 tion, newborn cells express the $\text{Na}^+\text{-K}^+\text{-2Cl}^-$ cotransporter NKCC1, which leads
55 to a high intracellular chloride concentration. Hence the GABA reversal potential
56 is higher than the resting potential (Ge et al., 2006; Heigele et al., 2016), and
57 GABAergic inputs lead to Cl^- ions outflow through the GABA_A ionic receptors,
58 which results in depolarization of the newborn cell (Ben-Ari, 2002; Owens and
59 Kriegstein, 2002). In the late phase of maturation, expression of the $\text{K}^+\text{-Cl}^-$ -
60 coupled cotransporter KCC2 kicks in, which lowers the intracellular chloride con-
61 centration of the newborn cell to levels similar to those of mature cells, leading
62 to a hyperpolarization of the cell membrane due to Cl^- inflow upon GABAergic
63 stimulation (Ben-Ari, 2002; Owens and Kriegstein, 2002). The transition from de-
64 polarizing (excitatory) to hyperpolarizing (inhibitory) effects of GABA is referred
65 to as the 'GABA-switch'. It has been shown that GABAergic inputs are crucial
66 for the integration of newborn DGCs into the preexisting circuit (Ge et al., 2006;
67 Chancey et al., 2013; Alvarez et al., 2016; Heigele et al., 2016).

68 The mammalian dentate gyrus contains – just like hippocampus in general –
69 a myriad of inhibitory cell types (Freund and Buzsáki, 1996; Somogyi and Klaus-

70 berger, 2005; Klausberger and Somogyi, 2008) including basket cells, chandelier
71 cells, and hilar cells. Basket cells can be subdivided in two categories: some ex-
72 press cholecystokinin (CCK) and vasoactive intestinal polypeptide (VIP), while
73 the others express parvalbumin (PV) and are fast-spiking (Freund and Buzsáki,
74 1996; Amaral et al., 2007). Chandelier cells also express PV (Freund and Buzsáki,
75 1996). Overall, it has been estimated that PV is expressed in 15-21% of all dentate
76 GABAergic cells (Freund and Buzsáki, 1996), and in 20-25% of the GABAergic
77 neurons in the granule cell layer (Houser, 2007). Amongst the GABAergic hilar
78 cells, 55% express somatostatin (SST) (Houser, 2007) [and somatostatin-positive
79 interneurons (SST-INs) represent about 16% of the GABAergic neurons in the
80 dentate gyrus as a whole (Freund and Buzsáki, 1996)]. While axons of hilar in-
81 terneurons (HIL) (Yuan et al., 2017) stay in the hilus and provide perisomatic inhi-
82 bition onto dentate GABAergic cells (Yuan et al., 2017), axons of hilar-perforant-
83 path-associated interneurons (HIPPA) extend to the molecular layer and provide
84 dendritic inhibition onto both DGCs and interneurons (Yuan et al., 2017). HIPPA
85 axons generate lots of synaptic terminals and extend as far as 3.5 mm along the
86 septotemporal axis of the dentate gyrus (Amaral et al., 2007). PV-expressing
87 interneurons (PV-INs) and SST-INs both target adult-born DGCs early (after
88 2-3 weeks) in their maturation (Groisman et al., 2020). PV-INs provide both
89 feedforward inhibition and feedback inhibition (also called lateral inhibition) to
90 the DGCs (Groisman et al., 2020). In general, SST-INs provide lateral, but not
91 feedforward, inhibition onto DGCs (Stefanelli et al., 2016; Groisman et al., 2020).

92 Adult-born DGCs are preferentially reactivated by stimuli similar to the ones
93 they experienced during their early phase of maturation, up to 3 weeks after cell
94 birth (Tashiro et al., 2007). Even though the amount of newly generated cells per
95 month is rather low (3 to 6% of the total DGCs population (Van Praag et al.,
96 1999; Cameron and McKay, 2001)), adult-born DGCs are critical for behavioral
97 pattern separation (Clelland et al., 2009; Sahay et al., 2011a; Jessberger et al.,
98 2009), in particular in tasks where similar stimuli or contexts have to be discrim-
99 inated (Clelland et al., 2009; Sahay et al., 2011a). However, the functional role
100 of adult-born DGCs is controversial (Sahay et al., 2011b; Aimone et al., 2011).
101 One view is that newborn DGCs contribute to pattern separation through a mod-
102 ulatory role (Sahay et al., 2011b). Another view suggests that newborn DGCs
103 act as encoding units that become sensitive to features of the environment which
104 they encounter during a critical window of maturation (Kee et al., 2007; Tashiro
105 et al., 2007). Some authors have even challenged the role of newborn DGCs in
106 pattern separation in the classical sense and have proposed a pattern integration
107 effect instead (Aimone et al., 2011). Within that broader controversy, we ask two
108 specific questions: First, why are GABAergic inputs crucial for the integration
109 of newborn DGCs into the preexisting circuit? And second, why are newborn
110 DGC particularly important in tasks where similar stimuli or contexts have to be
111 discriminated?

112 To address these questions, we present a model of how newborn DGCs inte-
113 grate into the preexisting circuit. In contrast to earlier models where synaptic
114 input connections onto newborn cells were assumed to be strong enough to drive
115 them (Chambers et al., 2004; Becker, 2005; Crick and Miranker, 2006; Wiskott
116 et al., 2006; Chambers and Conroy, 2007; Aimone et al., 2009; Appleby and
117 Wiskott, 2009; Weisz and Argibay, 2009, 2012; Temprana et al., 2015; Finnegan
118 and Becker, 2015; DeCostanzo et al., 2019), our model uses an unsupervised bi-
119 ologically plausible Hebbian learning rule that makes synaptic connections either
120 disappear or grow from small values at birth to values that eventually enable
121 feedforward input from EC to drive DGCs. Contrary to previous modeling stud-
122 ies, our plasticity model does not require an artificial renormalization of synaptic
123 connection weights since model weights are naturally bounded by homeostatic
124 heterosynaptic plasticity. We show that learning with a biologically plausible plas-
125 ticity rule is possible thanks to the GABA-switch, which has been overlooked in
126 previous modeling studies. Specifically the growth of synaptic weights from small
127 values is supported in our model by the excitatory action of GABA whereas, after
128 the switch, specialization of newborn cells arises from competition between DGCs,
129 triggered by the inhibitory action of GABA. Furthermore, our theory of adult-
130 born DGCs integration yields a transparent explanation of why newborn cells
131 favor pattern separation of similar stimuli, but do not impact pattern separation
132 of distinct stimuli.

133 Results

134 We model a small patch of cells within dentate gyrus as a recurrent network of 100
135 DGCs and 25 GABAergic interneurons, omitting the Mossy cells for the sake of
136 simplicity (Fig. 1b). The modeled interneurons correspond to SST-INs from the
137 HIPP category, as they are the providers of feedback inhibition to DGCs through
138 dendritic projections (Stefanelli et al., 2016; Yuan et al., 2017; Groisman et al.,
139 2020). The activity of a DGC with index i and an interneuron with index k is
140 described by their continuous firing rates ν_i and ν_k^I , respectively. Connectivity in
141 a localized patch of dentate neurons is high: DGCs densely project to GABAergic
142 interneurons (Acsády et al., 1998), and SST-INs heavily project to cells in their
143 neighborhood (Amaral et al., 2007). Hence, in the recurrent network model,
144 each model DGC projects to, and receives input from, a given interneuron with
145 probability 0.9. The exact percentage of GABAergic neurons (or SST-INs) in the
146 dentate gyrus as a whole is not known, but has been estimated at about 10% and
147 only a fraction of these are SST-INs (Freund and Buzsáki, 1996). The number of
148 inhibitory neurons in our model network might therefore seem too high. However,
149 our results are robust to substantial changes in the number of inhibitory neurons
150 (Suppl. Table S2).

151 Each of the 100 model DGCs receives input from a set of 144 model EC
152 cells (Fig. 1b). In the rat the number of DGCs has been estimated to be about
153 10^6 , while the number of EC input cells is estimated to be about $2 \cdot 10^5$ (An-
154 dersen et al., 2007), yielding an expansion factor from EC to dentate gyrus of
155 about 5. Theoretical analysis suggests that the expansion of the number of neu-
156 rons enhances decorrelation of the representation of input patterns (Marr, 1969;
157 Albus, 1971; Marr, 1971; Rolls and Treves, 1998), and promotes pattern sepa-
158 ration (Babadi and Sompolinsky, 2014). Our standard network model does not
159 reflect this expansion, because we want to highlight the particular ability of adult
160 neurogenesis in combination with the GABA-switch to decorrelate input patterns
161 independently of specific choices of the network architecture. However, we show
162 later that an enlarged network with an expansion from 144 model EC cells to 700
163 model DGCs (similar to the anatomical expansion factor) yields similar results.

164 At birth a DGC with index i does not receive synaptic glutamatergic input
165 yet. Hence the connection from any model EC cell with index j is initialized at
166 $w_{ij} = 0$. The growth or decay of the synaptic strength w_{ij} of the connection from
167 j to i is controlled by a Hebbian plasticity rule (Fig. 1c):

$$\Delta w_{ij} = \eta \{x_j \cdot \text{LTP}(\nu_i - \theta) - x_j \cdot \text{LTD}(\theta - \nu_i) - w_{ij} \cdot \text{HET}(\nu_i - \theta)\} \quad (1)$$

168 where x_j is the firing rate of the presynaptic EC neuron and η ('learning rate')
169 is the susceptibility of a cell to synaptic plasticity. The first term on the right-
170 hand-side of equation (1) describes Long-Term-Potential (LTP) whenever the
171 presynaptic neuron is active ($x_j > 0$) and the postsynaptic firing ν_i is above
172 a threshold θ ; the second term on the right-hand-side of equation (1) describes
173 Long-Term-Depression (LTD) whenever the presynaptic neuron is active and the
174 postsynaptic firing rate is positive but below the threshold θ ; LTD stops if the
175 synaptic weight is zero. Such a combination of LTP and LTD is consistent with
176 experimental data (Artola et al., 1990; Sjöström et al., 2001) as shown in ear-
177 lier rate-based (Bienenstock et al., 1982) or spike-based (Pfister and Gerstner,
178 2006) plasticity models. The third term on the right-hand-side of equation (1)
179 implements heterosynaptic (HET) plasticity (Chistiakova et al., 2014; Zenke and
180 Gerstner, 2017) whenever the postsynaptic neuron fires at a rate above θ , inde-
181 pendent of presynaptic activity (Methods). It ensures that the weights cannot
182 grow without bounds (Methods). Since survival of newborn cells requires NMDA
183 receptor activation (Tashiro et al., 2006), a DGC which has not been able to
184 grow several strong weights is removed after some time and replaced by another
185 newborn DGC.

186 We ask whether such a biologically-plausible plasticity rule enables adult-born
187 DGCs to be integrated in an existing network of mature cells. To address this
188 question, we exploit two observations (Fig. 1a): first, the effect of interneurons
189 onto newborn DGCs exhibits a GABA-switch from excitatory to inhibitory after
190 about three weeks of maturation (Ge et al., 2006; Deng et al., 2010) and, second,

191 newborn DGCs receive input from interneurons early in their maturation (before
192 the third week), but project back to interneurons only later (Temprana et al.,
193 2015). However, before integration of adult-born DGCs can be addressed, an
194 adult-stage network where mature cells already store some memories has to be
195 constructed.

196 **Mature neurons represent prototypical input patterns**

197 In an adult-stage network, some mature cells already have a functional role. Hence
198 we pretrain our network of 100 DGCs using the same learning rule (equation (1))
199 that we will use later for the integration of newborn cells. For the stimulation of
200 EC cells, we apply patterns representing thousands of handwritten digits in differ-
201 ent writing styles from MNIST, a standard data set in artificial intelligence (LeCun
202 et al., 1998). Even though we do not expect EC neurons to show a 2-dimensional
203 arrangement, the use of 2-dimensional patterns provides a simple way to visualize
204 the activity of all 144 EC neurons in our model (Fig. 1d). We implicitly model
205 feedforward inhibition from PV-INs (Groisman et al., 2020) by normalizing the
206 L2-norm of each input pattern to unity (Methods). Below, we present results
207 for a representative combination of three digits (digits 3, 4 and 5), but other
208 combinations of digits have also been tested (Suppl. Table S1).

209 After pretraining with patterns from digits 3 and 4 in a variety of writing styles,
210 we examine the receptive field of each DGC. Each receptive field, consisting of
211 the connections from all 144 EC neurons onto one DGC, is characterized by its
212 spatial structure (i.e., the pattern of connection weights) and its total strength
213 (i.e., the efficiency of the optimal stimulus to drive the cell). We observe that out
214 of the 100 DGCs, some have developed spatial receptive fields that correspond
215 to different writing styles of digit 3, others receptive fields that correspond to
216 variants of digit 4 (Fig. 1e).

217 Behavioral discrimination has been shown to be correlated with classification
218 accuracy based on DGC population activity (Woods et al., 2020). Hence, to quan-
219 tify the representation quality, we compute classification performance by a linear
220 classifier that is driven by the activity of our 100 DGC model cells (Methods). At
221 the end of pretraining, the classification performance for patterns of digits 3 and 4
222 from a distinct test set not used during pretraining is high: 99.25% (classification
223 performance on digit 3: 98.71%; digit 4: 99.80%), indicating that nearly all input
224 patterns of the two digits are well represented by the network of mature DGCs.
225 The median classification performance for ten random combinations of two groups
226 of pretrained digits is 98.54%, the 25th-percentile 97.26%, and the 75th-percentile
227 99.5% (Suppl. Table S1).

228 A detailed mathematical analysis (Methods) shows that heterosynaptic plas-

229 ticity in equation (1) ensures that the total strength of the receptive field of each
230 selective DGC converges to a stable value which is similar for selective DGCs.
231 As a consequence, synaptic weights are intrinsically bounded without the need to
232 impose hard bounds on the weight dynamics. Moreover, the spatial structure of
233 the receptive field represents the weighted average of all those input patterns for
234 which that DGC is responsive. The mathematical analysis also shows that those
235 DGCs that do not develop selectivity have weak synaptic connections and a very
236 low total strength of the receptive field.

237 **Newborn neurons become selective for novel patterns dur-** 238 **ing maturation**

239 After convergence of synaptic weights during pretraining, selective DGCs are con-
240 sidered mature cells. Some DGCs did not develop any strong weight patterns
241 and exhibit unselective receptive fields after pretraining (highlighted in red in
242 Fig. 1e). We classify these as unresponsive units. Since unresponsive model units
243 have weak synaptic connections, we assume them to die because of lack of NMDA
244 receptor activation (Tashiro et al., 2006), and replace them in the model by plastic
245 newborn DGCs. Mature cells are less plastic than newborn cells (Schmidt-Hieber
246 et al., 2004; Ge et al., 2007), so we set $\eta = 0$ in equation (1) for mature cells and
247 $\eta = 0.01$ for newborn cells. Feedforward connection weights from EC to mature
248 cells remain therefore fixed in our model. To mimic exposure of an animal to a
249 novel set of stimuli, we now add input patterns from digit 5 to the set of presented
250 stimuli, which was previously limited to patterns of digits 3 and 4.

251 We postulate that functional integration of newborn DGCs requires the two-
252 step maturation process caused by the GABA-switch from excitation to inhibition.
253 Since excitatory GABAergic input potentially increases correlated activity within
254 the dentate gyrus network, we predict that newborn DGCs respond to familiar
255 stimuli during the early phase of maturation, but not during the late phase, when
256 inhibitory GABAergic input leads to competition.

257 To test this hypothesis, our model newborn DGCs go through two maturation
258 phases (Methods). The early phase of maturation is cooperative because, for each
259 pattern presentation, activated mature DGCs indirectly excite the newborn DGCs
260 via GABAergic interneurons. We assume that in natural settings, this GABAergic
261 activation stays below the reversal potential of the GABA channels at which
262 shunting inhibition would be induced (Heigele et al., 2016). This lateral activation
263 of newborn DGCs drives the growth of their receptive fields in a direction similar
264 to those of the currently active mature DGCs. Consistent with our hypothesis
265 we find that, at the end of the early phase of maturation, newborn DGCs show a
266 receptive field corresponding to a mixture of several input patterns (Fig. 2a).

267 In the late phase of maturation, model newborn DGCs receive inhibitory
268 GABAergic input from interneurons, similar to the input received by mature
269 DGCs. Given that at the end of the early phase, newborn DGCs have receptive
270 fields similar to those of mature DGCs, lateral inhibition induces competition
271 with mature DGCs for activation during presentation of patterns from the novel
272 digit. Because model newborn DGCs start their late phase of maturation with a
273 higher excitability (lower threshold) compared to mature DGCs, consistent with
274 observed enhanced excitability of newborn cells (Schmidt-Hieber et al., 2004; Li
275 et al., 2017), the activation of newborn DGCs is facilitated for those input pat-
276 terns for which no mature DGC has preexisting selectivity. Therefore, in the late
277 phase of maturation, competition drives the synaptic weights of newborn DGCs
278 towards receptive fields corresponding to different subcategories of the ensemble
279 of input patterns of the novel digit 5 (Fig. 2b).

280 During maturation, the L2-norm of the feedforward weight vector onto new-
281 born DGCs increases (Fig. 2e) indicating an increase in total glutamatergic in-
282 nervation, e.g. through an increase in the number and size of spines (Zhao et al.,
283 2006). Nevertheless, the distribution of firing rates of newborn DGCs is shifted to
284 lower values at the end of the late phase compared to the end of the early phase of
285 maturation (Fig. 2c,d), consistent with in vivo calcium imaging recordings show-
286 ing that adult-born DGCs are more active than mature DGCs (Danielson et al.,
287 2016).

288 We emphasize that upon presentation of a pattern of a given digit, only those
289 DGCs with a receptive field similar to the specific writing style of the presented
290 pattern become strongly active, others fire at a medium firing rate, yet others at a
291 low rate (Fig. 2g). As a consequence, the firing rate of a particular newborn DGC
292 at the end of its maturation to a pattern from digit 5 is strongly modulated by the
293 specific choice of stimulation pattern within the class of '5's. Analogous results
294 are obtained for patterns from pretrained digits 3 and 4 (Suppl. Fig S1). Hence,
295 the ensemble of DGCs is effectively performing pattern separation *within* each
296 digit class as opposed to a simple ternary classification task. The selectivity of
297 newborn DGCs develops during maturation. Indeed, during the late, competitive,
298 phase, the percentage of active newborn DGCs decreases, both upon presentation
299 of familiar patterns (digits 3 and 4), as well as upon presentation of novel pat-
300 terns (digit 5) (Fig. 2f). This reflects the development of the selectivity of our
301 model newborn DGCs from broad to narrow tuning, consistent with experimental
302 observations (Marín-Burgin et al., 2012; Danielson et al., 2016).

303 **Adult-born neurons promote better discrimination**

304 As above, we compute classification performance of our model network as a sur-
305rogate for behavioral discrimination (Woods et al., 2020). At the end of the late

306 phase of maturation of newborn DGCs, we obtain an overall classification perfor-
307 mance of 94.56% for the three ensembles of digits (classification performance for
308 digit 3: 90.50%; digit 4: 98.17%; digit 5: 95.18%). Confusion matrices show that
309 although novel patterns are not well classified at the end of the early phase of
310 maturation (Fig. 3e), they are as well classified as pretrained patterns at the end
311 of the late phase of maturation (Fig. 3f).

312 We compare this performance with that of a network where all three digit
313 ensembles are simultaneously pretrained (Fig. 3a, control 1). In this case, the
314 overall classification performance is 92.09% (classification performance for digit 3:
315 86.83%; digit 4: 98.78%; digit 5: 90.70%). The confusion matrix show that
316 all three digits are decently classified, but with an overall lower performance
317 (Fig. 3d). Across ten simulation experiments, classification performance is sig-
318 nificantly higher when a novel ensemble of patterns is learned sequentially by
319 newborn DGCs, than if all patterns are learned simultaneously (Wilcoxon signed
320 rank test: p-val = 0.0020, Wilcoxon signed rank = 55; one-way t-test: p-val =
321 0.0269, t-stat = 2.6401, df = 9; Suppl. Table S1).

322 Furthermore, if two novel ensembles of digits (instead of a single one) are
323 introduced during maturation of newborn DGCs, we observe that some newborn
324 DGCs become selective for one of the novel digits, while others become selective for
325 the other novel digit (Suppl. Fig. S2a). This was expected, since we have found
326 earlier that DGCs are becoming selective for different prototype writing styles
327 even *within* a digit category; hence introducing several additional digit categories
328 of novel patterns simply increases the prototype diversity. Therefore, newborn
329 DGCs can ultimately promote separation of several novel overarching categories
330 of patterns, no matter if they are learned simultaneously or sequentially (Suppl.
331 Fig. S2b).

332 **The GABA-switch guides learning of novel representations**

333 To assess whether maturation of newborn DGCs promotes learning of a novel
334 ensemble of digit patterns, we compare our results with a control model without
335 neurogenesis (control 2). Similar to the neurogenesis case, patterns from the novel
336 digit 5 are introduced after pretraining with patterns from digits 3 and 4. The
337 feedforward weights and thresholds of DGCs that developed selectivity during
338 pretraining are fixed (learning rate $\eta = 0$), while the thresholds and weights of
339 all unresponsive neurons remain plastic after pretraining ($\eta = 0.01$). The only
340 differences to the model with neurogenesis are that in the control case unresponsive
341 neurons: (i) keep their feedforward weights (i.e., no reinitialization to low values),
342 and (ii) keep the same connections from and to inhibitory neurons.

343 We find that without neurogenesis, the previously unresponsive DGCs do not

344 become selective for the novel digit 5, no matter during how many epochs pat-
345 terns are presented (we went up to 100 epochs) (Fig. 3b, control 2). Therefore,
346 if patterns from digit 5 are presented to the network, the model fails to discrim-
347 inate them from the previously learned digits 3 and 4: the overall classification
348 performance is 81.69% (classification performance for digit 3: 85.94%; digit 4:
349 97.56%; digit 5: 59.42%). This result suggests that integration of newborn DGCs
350 is beneficial for sequential learning of novel patterns.

351 As a further control (control 3), we compare with a model where all DGCs
352 keep plastic feedforward weights at the end of pretraining and upon introduction
353 of the novel digit 5, no matter if they became selective or not for the pretrained
354 digits 3 and 4. We observe that in the case where all neurons are plastic, learning
355 of the novel digit occurs at the cost of loss of selectivity of mature neurons. Several
356 DGCs switch their selectivity to become sensitive to the novel digit (Fig. 3c), while
357 none of the previously unresponsive units becomes selective for presented patterns
358 (compare with Fig. 1e). In contrast to the model with neurogenesis, we observe a
359 drop in classification performance to 90.92% (classification performance for digit
360 3: 85.45%; digit 4: 98.37%; digit 5: 88.90%). We find that the classification
361 performance for digit 3 is the one which decreases the most. This is due to the
362 fact that many DGCs previously selective for digit 3 modified their weights to
363 become selective for digit 5. Importantly, the more novel patterns are introduced,
364 the more overwriting of previously stored memories occurs. Hence, if all DGCs
365 remain plastic, discrimination between a novel pattern and a familiar pattern
366 stored long ago is impaired.

367 **Maturation of newborn neurons shapes the representation** 368 **of novel patterns**

369 Since each input pattern stimulates slightly different, yet overlapping, subsets of
370 the 100 model DGCs in a sparse code such that about 20 DGCs respond to each
371 pattern (Fig. 2g), there is no simple one-to-one assignment between neurons and
372 patterns. In order to visualize the activity patterns of the ensemble of DGCs, we
373 perform dimensionality reduction. We construct a two-dimensional space using
374 the activity patterns of the network at the end of the late phase of maturation
375 of newborn DGCs trained with '3's, '4's and '5's. One axis connects the center
376 of mass (in the 100-dimensional activity space) of all DGC responses to '3's with
377 all responses to '5's (arbitrarily called 'axis 1') and the other axis those from '4's
378 to '5's (arbitrarily called 'axis 2'). We then project the activity of the 100 model
379 DGCs upon presentation of MNIST testing patterns onto those two axes, both at
380 the end of the early and late phase of maturation of newborn DGCs (Methods).
381 Each 2-dimensional projection is illustrated by a dot whose color corresponds to
382 the digit class of the presented input pattern (blue for digit 3, green for digit 4,

383 red for digit 5). Different input patterns within the same digit class cause different
384 activation patterns of the DGCs, as depicted by extended clouds of dots of the
385 same color (Fig. 4a,b). Interestingly, an example pattern of a '5' that is visually
386 similar to a '4' (characterized by the green cross) yields a DGC representation
387 that lies closer to other '4's (green cloud of dots) than to typical '5's (red cloud of
388 dots) (Fig. 4b). Noteworthy the separation of the representation of '5's from '3's
389 and '4's is better at end of the late phase (Fig. 4b) when compared to the end of
390 the early phase of maturation (Fig. 4a). For instance, even though the pattern
391 '5' corresponding to the orange cross is represented close to representations of '4's
392 at the end of the early phase of maturation (green cloud of dots, Fig. 4a), it is
393 represented far from any '3's and '4's at the end of maturation (Fig. 4b). The
394 expansion of the representation of '5's into a previously empty subspace evolves
395 as a function of time during the late phase of maturation (Fig. 4d).

396 **Robustness of the model**

397 Our results are robust to changes in network architecture. As mentioned earlier,
398 neither the exact number of GABAergic neurons (Suppl. Table S2), nor that of
399 DGCs is critical. Indeed, a larger network with 700 DGCs, thus mimicking the
400 anatomically observed expansion factor of about 5 between EC and dentate gyrus
401 (all other parameters unchanged), yields similar results (Suppl. Table S3).

402 In the network with 700 DGCs, 275 cells remain unresponsive after pretrain-
403 ing with digits 3 and 4. In line with our earlier approach in the network with
404 100 DGCs, we can algorithmically replace all unresponsive neurons with newborn
405 DGCs before patterns of digit 5 are added. Upon maturation, newborn DGC
406 receptive fields provide a detailed representation of the prototypes of the novel
407 digit 5 (Suppl. Fig. S4) and good classification performance is obtained (Suppl.
408 Table S3). Interestingly, due to the randomness of the recurrent connections,
409 some newborn DGCs become selective for particular prototypes of the familiar
410 (pretrained) digits that are not already extensively represented by the network
411 (see newborn DGCs selective for digit 4 highlighted by magenta squares in Suppl.
412 Fig. S4).

413 As an alternative to replacing all unresponsive cells simultaneously, we can also
414 replace only a fraction of them by newborn cells so as to simulate a continuous
415 turn-over of cells. For example, if 119 of the 275 unresponsive cells are replaced
416 by newborn DGCs before the start of presentations of digit 5, then these 119
417 cells become selective for different writing styles and generic features of the novel
418 digit 5 (Suppl. Fig. S5) and allow a good classification performance of all three
419 digits. On the other hand, replacing only 35 of the 275 unresponsive cells is not
420 sufficient (Suppl. Table S3). In an even bigger network with more than 144
421 EC cells and more than 700 DGCs, we could choose to replace 1% of the total

422 DGC population per week by newborn cells, consistent with biology (Van Praag
423 et al., 1999; Cameron and McKay, 2001). Importantly, if only a small fraction
424 of unresponsive cells are replaced at a given moment, other unresponsive cells
425 remain available to be replaced later by newborn DGCs that are then ready to
426 learn new stimuli.

427 Interestingly, the timing of the introduction of the novel stimulus is impor-
428 tant. In our standard neurogenesis model, we introduce the novel digit 5 at
429 the beginning of the early phase of maturation, which consists in one epoch of
430 MNIST training patterns (all patterns are presented once). For the network with
431 100 DGCs, if the novel digit is only introduced in the middle of the early phase
432 (half epoch), it cannot be properly learned (classification performance for digit
433 5: 46.52%). However, if introduced after three-eighths or one-quarter of the early
434 phase, the novel digit can be picked out (classification performance for digit 5:
435 93.61% and 94.17% resp.). We thus observe an increase in performance the ear-
436 lier the novel digit is introduced (classification performance for digit 5 was 95.18%
437 when introduced at the beginning of the early phase of maturation). Therefore
438 our model predicts that a novel stimulus has to be introduced early enough with
439 respect to newborn DGC maturation to be well discriminated, and that the ac-
440 curacy of discrimination is better the earlier it is introduced. This could lead
441 to an online scenario of our model, where adult-born DGCs are produced every
442 day and different classes of novel patterns are introduced at different timepoints.
443 Then different model newborn DGCs would become selective for different novel
444 patterns according to their maturation stage with respect to presentation of the
445 novel patterns.

446 **Newborn dentate granule cells become selective for similar** 447 **novel patterns**

448 To investigate whether our theory for integration of newborn DGCs can explain
449 why adult dentate gyrus neurogenesis promotes discrimination of similar stimuli,
450 but does not affect discrimination of distinct patterns (Clelland et al., 2009; Sahay
451 et al., 2011a), we use a simplified competitive winner-take-all network (Methods).
452 It contains only as many DGCs as trained clusters, and the GABAergic inhibitory
453 neurons are implicitly modeled through direct DGC-to-DGC inhibitory connec-
454 tions. DGCs are either silent or active (binary activity state, while in the detailed
455 network DGCs had continuous firing rates). The synaptic plasticity rule is however
456 the same as for the detailed network, with different parameter values (Methods).
457 We also construct an artificial data set (Fig. 5a,b) that allows us to control the
458 similarity s of pairs of clusters (Methods). The MNIST data set is not appropri-
459 ate to distinguish similar from dissimilar patterns, because all digit clusters are
460 similar and highly overlapping, reflected by a high within cluster dispersion (e.g.

461 across the set of all '3') compared to the separation between clusters (e.g. typical
462 '3' versus typical '5').

463 After a pretraining period, a first mature DGC responds to patterns of cluster 1
464 and a second mature DGC to those of cluster 2 (Fig. 5e,f). We then fix the
465 feedforward weights of those two DGCs and introduce a newborn DGC in the
466 network. Thereafter, we present patterns from three clusters (the two pretrained
467 ones, as well as a novel one), while the plastic feedforward weights of the newborn
468 DGC are the only ones that are updated. We observe that the newborn DGC
469 ultimately becomes selective for the novel cluster if it is similar ($s = 0.8$) to
470 the two pretrained clusters (Fig. 5i), but not if it is distinct ($s = 0.2$, Fig. 5j).
471 The selectivity develops in two phases. In the early phase of maturation of the
472 newborn model cell, a pattern from the novel cluster that is similar to one of the
473 pretrained clusters activates the mature DGC that has a receptive field closest
474 to the novel pattern. The activated mature DGC drives the newborn DGC via
475 lateral excitatory GABAergic connections to a firing rate where LTP is triggered
476 at active synapses onto the newborn DGC. LTP also happens when a pattern
477 from one of the pretrained clusters is presented. Thus, synaptic plasticity leads
478 to a receptive field that reflects the average of all stimuli from all three clusters
479 (Fig. 5g).

480 To summarize our findings in a more mathematical language, we characterize
481 the receptive field of the newborn cell by the vector of its feedforward weights.
482 Analogous to the notion of a firing rate vector that represents the set of firing
483 rates of an ensemble of neurons, the feedforward weight vector represents the set
484 of weights of all synapses projecting onto a given neuron (Fig. 1b). In the early
485 phase of maturation, for similar clusters, the feedforward weight vector onto the
486 newborn DGC grows in the direction of the center of mass of all three clusters
487 (the two pretrained ones and the novel one), because for each pattern presentation
488 one of the mature DGCs becomes active (compare Fig. 5g and Fig. 5k). However,
489 if the novel cluster has a low similarity to pretrained clusters, patterns from the
490 novel cluster do not activate any of the mature DGCs. Therefore the receptive
491 field of the newborn cell reflects the average of stimuli from the two pretrained
492 clusters only (compare Fig. 5h and Fig. 5l).

493 As a result of the different orientation of the feedforward weight vector onto the
494 newborn DGC at the end of the early phase of maturation, two different situations
495 arise in the late phase of maturation, when lateral GABAergic connections are
496 inhibitory. If the novel cluster is similar to the pretrained clusters, the weight
497 vector onto the newborn DGC at the end of the early phase of maturation lies at
498 the center of mass of all the patterns across the three clusters. Thus it is closer to
499 the novel cluster than the weight vector onto either of the mature DGCs (Fig. 5g).
500 So if a novel pattern is presented, the newborn DGC wins the competition between
501 the three DGCs, and its feedforward weight vector moves towards the center of

502 mass of the novel cluster (Fig. 5i). By contrast, if the novel cluster is distinct, the
503 weight vector onto the newborn DGC at the end of the early phase of maturation
504 is located at the center of mass of the two pretrained clusters (Fig. 5h). If a novel
505 pattern is presented, no output unit is activated since their receptive fields are not
506 similar enough to the input pattern. Therefore the newborn DGC always stays
507 silent and does not update its feedforward weights (Fig. 5j). These results are
508 consistent with studies that have suggested that dentate gyrus is only involved
509 in the discrimination of similar stimuli, but not distinct stimuli (Gilbert et al.,
510 2001; Hunsaker and Kesner, 2008). For discrimination of distinct stimuli, another
511 pathway might be used, such as the direct EC to CA3 connection (Yeckel and
512 Berger, 1990; Fyhn et al., 2007).

513 In conclusion, our model suggests that adult dentate gyrus neurogenesis pro-
514 motes discrimination of similar patterns because newborn DGCs can ultimately
515 become selective for novel stimuli which are similar to already learned stimuli.
516 On the other hand, newborn DGCs fail to represent novel distinct stimuli, pre-
517 cisely because they are too distinct from other stimuli already represented by the
518 network. Presentation of novel distinct stimuli in the late phase of maturation
519 therefore does not induce synaptic plasticity of the newborn DGC feedforward
520 weight vector toward the novel stimuli. In the simplified network, the transition
521 between similar and distinct can be determined analytically (Methods). This anal-
522 ysis clarifies the importance of the switch from cooperative dynamics (excitatory
523 interactions) in the early phase to competitive dynamics (inhibitory interactions)
524 in the late phase of maturation.

525 **Upon successful integration the receptive field of a newborn** 526 **DGC represents an average of novel stimuli**

527 With the simplified model network, it is possible to analytically compute the
528 maximal strength of the DGC receptive field via the L2-norm of the feedforward
529 weight vector onto the newborn DGC (Suppl. Material). In addition, the angle
530 between the center of mass of the novel patterns and the feedforward weight vector
531 onto the adult-born DGC can also be analytically computed (Suppl. Material).
532 To illustrate the analytical results and characterize the evolution of the receptive
533 field of the newborn DGC, we thus examine the angle ϕ of the feedforward weight
534 vector with the center of mass of the novel cluster (i.e. the average of the novel
535 stimuli), as a function of maturation time (Fig. 6b,c and Suppl. Fig. S3).

536 In the early phase of maturation, the feedforward weight vector onto the new-
537 born DGC grows, while its angle with the center of mass of the novel cluster stays
538 constant (Suppl. Fig. S3). In the late phase of maturation, the angle ϕ between
539 the center of mass of the novel cluster and the feedforward weight vector onto the

540 newborn DGC decreases in the case of similar patterns (Fig. 6c, Suppl. Fig. S3),
541 but not in the case of distinct patterns (Suppl. Fig. S3), indicating that the new-
542 born DGC becomes selective for the novel cluster for similar but not for distinct
543 patterns.

544 The analysis of the simplified model thus leads to a geometric picture that
545 helps us to understand how the similarity of patterns influences the evolution of
546 the receptive field of the newborn DGC before and after the switch from excitation
547 to inhibition of the GABAergic input. For novel patterns that are similar to known
548 patterns, the receptive field of a newborn DGC at the end of maturation represents
549 the average of novel stimuli.

550 Discussion

551 While experimental studies, such as manipulating the ratio of NKCC1 to KCC2,
552 suggest that the switch from excitation to inhibition of the GABAergic input onto
553 adult-born DGCs is crucial for their integration into the preexisting circuit (Ge
554 et al., 2006; Alvarez et al., 2016) and that adult dentate gyrus neurogenesis pro-
555 motes pattern separation (Clelland et al., 2009; Sahay et al., 2011a; Jessberger
556 et al., 2009), the link between channel properties and behavior has remained puz-
557 zling (Sahay et al., 2011b; Aimone et al., 2011). Our modeling work shows that
558 the GABA-switch enables newborn DGCs to become selective for novel stimuli
559 which are similar to familiar, already stored, representations, consistent with the
560 experimentally-observed function of pattern separation (Clelland et al., 2009; Sa-
561 hay et al., 2011a; Jessberger et al., 2009).

562 Previous modeling studies already suggested that newborn DGCs integrate
563 novel inputs into the representation in dentate gyrus (Chambers et al., 2004;
564 Becker, 2005; Crick and Miranker, 2006; Wiskott et al., 2006; Chambers and Con-
565 roy, 2007; Appleby and Wiskott, 2009; Aimone et al., 2009; Weisz and Argibay,
566 2009, 2012; Temprana et al., 2015; Finnegan and Becker, 2015; DeCostanzo et al.,
567 2019). However, our work differs from them in four important aspects. First
568 of all, we implement an unsupervised biologically plausible plasticity rule, while
569 many studies used supervised algorithmic learning rules (Chambers et al., 2004;
570 Becker, 2005; Chambers and Conroy, 2007; Weisz and Argibay, 2009; Finnegan
571 and Becker, 2015; DeCostanzo et al., 2019). Second, as we model the formerly
572 neglected GABA-switch, the connection weights from EC to newborn DGCs are
573 grown from small values through cooperativity in the early phase of maturation.
574 This integration step was mostly bypassed in earlier models by initialization of
575 the connectivity weights towards newborn DGCs to random, yet fully grown val-
576 ues (Crick and Miranker, 2006; Aimone et al., 2009; Weisz and Argibay, 2009,
577 2012; Finnegan and Becker, 2015). Third, as the dentate gyrus network is com-

578 monly modeled as a competitive network, weight normalization is crucial. In our
579 framework, competition occurs during the late phase of maturation. Previous
580 modeling works either applied algorithmic weight normalization or hard bounds
581 on the weights at each iteration step (Crick and Miranker, 2006; Aimone et al.,
582 2009; Weisz and Argibay, 2009, 2012; Temprana et al., 2015; Finnegan and Becker,
583 2015). Instead, our plasticity rule includes heterosynaptic plasticity which intrinsi-
584 cally softly bounds connectivity weights by a homeostatic effect. Finally, although
585 some earlier computational models of adult dentate gyrus neurogenesis could ex-
586 plain the pattern separation abilities of newborn cells, separation was obtained
587 independently of the similarity between the stimuli. Contrarily to experimental
588 data, no distinction was made between similar and distinct patterns (Chambers
589 et al., 2004; Becker, 2005; Crick and Miranker, 2006; Wiskott et al., 2006; Cham-
590 bers and Conroy, 2007; Aimone et al., 2009; Appleby and Wiskott, 2009; Weisz and
591 Argibay, 2012; Temprana et al., 2015; Finnegan and Becker, 2015; DeCostanzo
592 et al., 2019). To our knowledge, we present the first model that can explain both:
593 (i) how adult-born DGCs integrate into the preexisting network, and (ii) why they
594 promote pattern separation of similar stimuli and not distinct stimuli.

595 Our work emphasizes why a two-phase maturation of newborn DGCs is ben-
596 efcial for proper integration in the preexisting network. From a computational
597 perspective, the early phase of maturation, when GABAergic inputs onto newborn
598 DGCs are excitatory, corresponds to cooperative unsupervised learning. There-
599 fore, the synapses grow in the direction of patterns that indirectly activate the
600 newborn DGCs via GABAergic interneurons (Fig. 6a). At the end of the early
601 phase of maturation, the receptive field of a newborn DGC represents the center
602 of mass of all input patterns that led to its (indirect) activation. In the late phase
603 of maturation, GABAergic inputs onto newborn DGCs become inhibitory, so that
604 lateral interactions change from cooperation to competition, causing a shift of the
605 receptive fields of the newborn DGCs towards novel features (Fig. 6b). At the end
606 of maturation, newborn DGCs are thus selective for novel inputs. This integra-
607 tion mechanism is in agreement with the experimental observation that newborn
608 DGCs are broadly tuned early in maturation, yet highly selective at the end of
609 maturation (Marín-Burgin et al., 2012; Danielson et al., 2016). Loosely speaking,
610 the cooperative phase of excitatory GABAergic input promotes the growth of the
611 synaptic weights coarsely in the relevant direction, whereas the competitive phase
612 of inhibitory GABAergic input helps to specialize on detailed, but potentially
613 important differences between patterns.

614 In the context of theories of unsupervised learning, the switch of lateral GABAer-
615 gic input to newborn DGCs from excitatory to inhibitory provides a biological
616 solution to the “problem of unresponsive units” (Hertz et al., 1991). Unsuper-
617 vised competitive learning has been used to perform clustering of input patterns
618 into a few categories (Rumelhart and Zipser, 1985; Grossberg, 1987; Kohonen,
619 1989; Hertz et al., 1991; Du, 2010). Ideally, after learning of the feedforward

620 weights between an input layer and a competitive network, input patterns that
621 are distinct from each other activate different neuron assemblies of the competi-
622 tive network. After convergence of competitive Hebbian learning, the vector of
623 feedforward weights onto a given neuron points to the center of mass of the cluster
624 of input patterns for which it is selective (Kohonen, 1989; Hertz et al., 1991).
625 Yet, if the synaptic weights are randomly initialized, it is possible that the set
626 of feedforward weights onto some neurons of the competitive network point in a
627 direction “quasi-orthogonal” (Methods) to the subspace of the presented input
628 patterns. Therefore those neurons, called “unresponsive units”, will never get
629 active during pattern presentation. Different learning strategies have been devel-
630 oped in the field of artificial neural networks to avoid this problem (Grossberg,
631 1976; Bienenstock et al., 1982; Rumelhart and Zipser, 1985; Grossberg, 1987; De-
632 Sieno, 1988; Kohonen, 1989; Hertz et al., 1991; Du, 2010). However, most of
633 these algorithmic approaches lack a biological interpretation. In our model, weak
634 synapses onto newborn DGCs form spontaneously after neuronal birth. The exci-
635 tatory GABAergic input in the early phase of maturation drives the growth of the
636 synaptic weights in the direction of the subspace of presented patterns that suc-
637 ceed in activating some of the mature DGCs. Hence the early cooperative phase
638 of maturation can be seen as a smart initialization of the synaptic weights onto
639 newborn DGCs, close enough to novel patterns so as to become selective for them
640 in the late competitive phase of maturation. However, the cooperative phase is
641 helpful only if the novel patterns are similar to the input statistics defined by the
642 set of known (familiar) patterns.

643 Our results are in line with the classic view that dentate gyrus is responsible
644 for decorrelation of inputs (Marr, 1969; Albus, 1971; Marr, 1971; Rolls and Treves,
645 1998), a necessary step for differential storage of similar memories in CA3, and
646 with the observation that dentate gyrus lesions impair discrimination of similar
647 but not distinct stimuli (Gilbert et al., 2001; Hunsaker and Kesner, 2008). To
648 discriminate distinct stimuli, another pathway might be involved, such as the
649 direct EC to CA3 connection (Yeckel and Berger, 1990; Fyhn et al., 2007).

650 Our model of transition from an early cooperative phase to a late competi-
651 tive phase makes specific predictions, at the behavioral and cellular level. In
652 our model, the early cooperative phase of maturation can only drive the growth
653 of synaptic weights onto newborn cells if they are indirectly activated by ma-
654 ture DGCs through GABAergic input, which has an excitatory effect due to the
655 high NKCC1/KCC2 ratio early in maturation. Therefore our model predicts that
656 NKCC1-knockout mice would be impaired in discriminating similar contexts or
657 objects because newborn cells stay silent due to lack of indirect activation. The
658 feedforward weight vector onto newborn DGCs could not grow in the early phase
659 and newborn DGCs could not become selective for novel inputs. Therefore our
660 model predicts that since newborn DGCs are poorly integrated into the preex-
661 isting circuit, they are unlikely to survive. If, however, in the same paradigm

662 newborn cells are activated by light-induced or electrical stimulation, we predict
663 that they become selective to novel patterns. Thus discrimination abilities would
664 be restored and newborn DGCs are likely to survive. Analogously, we predict that
665 using inducible NKCC1-knockout mice, animals would gradually be impaired in
666 discrimination tasks after induced knockout and reach a stable maximum impair-
667 ment about 3 weeks after the start of induced knockout.

668 Experimental observations support the importance of the switch from early
669 excitation to late inhibition of the GABAergic input onto newborn DGCs. An ab-
670 sence of early excitation using NKCC1-knockout mice has been shown to strongly
671 affect synapse formation and dendritic development *in vivo* (Ge et al., 2006). Con-
672 versely, a reduction in inhibition in the dentate gyrus through decrease in KCC2
673 expression has been associated with epileptic activity (Pathak et al., 2007; Bar-
674 mashenko et al., 2011). An analogous switch of the GABAergic input has been
675 observed during development, and its proper timing has been shown to be cru-
676 cial for sensorimotor gating and cognition (Wang and Kriegstein, 2010; Furukawa
677 et al., 2017). In addition to early excitation and late inhibition, our theory also
678 critically depends on the switch. In our model, the switch makes an instantaneous
679 transition between early and late phase of maturation. Several experimental re-
680 sults have suggested that the switch is indeed sharp and occurs within a single
681 day, both during development (Khazipov et al., 2004; Tyzio et al., 2007; Leonzino
682 et al., 2016) and adult dentate gyrus neurogenesis (Heigele et al., 2016). Fur-
683 thermore, in hippocampal cell cultures, expression of KCC2 is upregulated by
684 GABAergic activity but not affected by glutamatergic activity (Ganguly et al.,
685 2001). A similar process during adult dentate gyrus neurogenesis would increase
686 the number of newborn DGCs available for representing novel features by advanc-
687 ing the timing of their switch. In this way, instead of a few thousands of newborn
688 DGCs ready to switch (3 to 6% of the whole population (Van Praag et al., 1999;
689 Cameron and McKay, 2001), divided by 30 days), a larger fraction of newborn
690 DGCs would be made available for coding, if appropriate stimulation occurs.

691 To conclude, our theory for integration of adult-born DGCs suggests that
692 newborn cells have a coding –rather than a modulatory– role during dentate gyrus
693 pattern separation function. Our theory highlights the importance of GABAergic
694 input in adult dentate gyrus neurogenesis, and links the switch from excitation
695 to inhibition to the integration of newborn DGCs into the preexisting circuit.
696 Finally, it illustrates how Hebbian plasticity of EC to DGC synapses along with
697 the switch make newborn cells suitable to promote pattern separation of similar
698 but not distinct stimuli, a long-standing mystery in the field of adult dentate
699 gyrus neurogenesis (Sahay et al., 2011b; Aimone et al., 2011).

700 Methods

701 Network architecture and neuronal dynamics

702 DGCs are the principal cells of the dentate gyrus. They mainly receive excitatory
703 projections from the entorhinal cortex through the perforant path and GABAergic
704 inputs from local interneurons, as well as excitatory input from Mossy cells. They
705 project to CA3 pyramidal cells and inhibitory neurons, as well as local Mossy
706 cells (Acsády et al., 1998; Henze et al., 2002; Amaral et al., 2007; Temprana
707 et al., 2015). In our model, we omit Mossy cells for simplicity and describe the
708 dentate gyrus as a competitive circuit consisting of N_{DGC} dentate granule cells
709 and N_I GABAergic interneurons (Fig. 1b). The activity of N_{EC} neurons in EC
710 represents an input pattern $\vec{x} = (x_1, x_2, \dots, x_{N_{EC}})$. Because the perforant path
711 also induces strong feedforward inhibition in the dentate gyrus (Li et al., 2013),
712 we assume that the effective EC activity is normalized, such that $\|\vec{x}\| = 1$ for
713 any input pattern \vec{x} . We use P different input patterns \vec{x}^μ , $1 \leq \mu \leq P$ in the
714 simulations of the model.

715 In our network, model EC neurons have excitatory all-to-all connections to
716 the DGCs. In rodent hippocampus, spiking mature DGCs activate interneurons
717 in DG, which in turn inhibit other mature DGCs (Temprana et al., 2015; Alvarez
718 et al., 2016). In our model, the DGCs are thus recurrently connected with in-
719 hibitory neurons (Fig. 1b). Connections from DGCs to interneurons exist in our
720 model with probability p_{IE} and have a weight w_{IE} . Similarly, connections from
721 interneurons to DGCs occur with probability p_{EI} and have a weight w_{EI} . All
722 parameters are reported in Table 1 (Biologically-plausible network).

723 Before an input pattern is presented, all rates of model DGCs are initialized to
724 zero. Upon stimulation with input pattern \vec{x} , the firing rate ν_i of DGC i evolves
725 according to (Miller and Fumarola, 2012):

$$\tau_m \frac{d\nu_i}{dt} = -\nu_i + \tanh\left(\frac{[I_i - b_i]_+}{L}\right) \quad (2)$$

726 where $[.]_+$ denotes rectification: $[a] = a$ for $a > 0$ and zero otherwise. Here, b_i is
727 a firing threshold, $L = 0.5$ is the smoothness parameter of the frequency-current
728 curve (L^{-1} is the slope of the frequency-current curve at the firing threshold), and
729 I_i the total input to cell i :

$$I_i = \sum_{j=1}^{N_{EC}} w_{ij} x_j + \sum_{k=1}^{N_I} w_{ik}^{EI} \nu_k^I \quad (3)$$

730 with x_j the activity of EC input neuron j , $w_{ij} \geq 0$ the feedforward weight from
731 EC input neuron j to DGC i , and w_{ik}^{EI} the weight from inhibitory neuron k to

732 DGC i . The sum runs over all inhibitory neurons, but the weights are set to
 733 $w_{ik}^{EI} = 0$ if the connection is absent. The firing rate ν_i is unit-free and normalized
 734 to a maximum of 1, which we interpret as a firing rate of 10 Hz. We take the
 735 synaptic weights as unit-less parameters such that I_i is also unit-free.

736 The firing rate ν_k^I of inhibitory neuron k , is defined as:

$$\tau_{\text{inh}} \frac{d\nu_k^I}{dt} = -\nu_k^I + [I_k^I - p^* N_{DGC}]_+ \quad (4)$$

737 with p^* a parameter which relates to the desired ensemble sparsity, and I_k^I the
 738 total input towards interneuron k , given as:

$$I_k^I = \sum_{i=1}^{N_{DGC}} w_{ki}^{IE} \nu_i \quad (5)$$

739 with w_{ki}^{IE} the weight from DGC i to inhibitory neuron k . (We set $w_{ki}^{IE} = 0$ if
 740 the connection is absent.) The feedback from inhibitory neurons ensures a sparse
 741 activity of model DGCs for each pattern. With $p^* = 0.1$ we find that more than 70
 742 % of model DGCs are silent (firing rate < 1 Hz (Senzai and Buzsáki, 2017)) when
 743 an input pattern is presented, and less than 10% are highly active (firing rate
 744 > 9 Hz) (Fig. 2c,d), consistent with the experimentally observed sparse activity
 745 in dentate gyrus (Chawla et al., 2005).

746 Plasticity rule

Projections from EC onto newborn DGCs exhibit Hebbian plasticity (Schmidt-Hieber et al., 2004; Ge et al., 2007; McHugh et al., 2007). Therefore, in our model the connections from EC neurons to DGCs are plastic, following a Hebbian learning rule which exhibits long-term depression (LTD) or long-term potentiation (LTP) depending on the firing rate ν_i of the postsynaptic cell (Bienenstock et al., 1982; Artola et al., 1990; Sjöström et al., 2001; Pfister and Gerstner, 2006). Input patterns \vec{x}^μ , $1 \leq \mu \leq P$, are presented in random order. For each input pattern, we let the firing rates converge for a time T where T was chosen long enough to achieve convergence to a precision of 10^{-6} . After $n - 1$ presentations (i.e. at time $(n - 1) \cdot T$) the weight vector has value $w_{ij}^{(n-1)}$. We then present the next pattern and update at time $n \cdot T$ ($w_{ij}^{(n)} = w_{ij}^{(n-1)} + \Delta w_{ij}$), according to the following plasticity rule:

$$\Delta w_{ij} = \eta \{ -\alpha x_j \nu_i [\theta - \nu_i]_+ + \gamma x_j \nu_i [\nu_i - \theta]_+ - \beta w_{ij} [\nu_i - \theta]_+ \nu_i^3 \} \quad (6)$$

747 where x_j is the firing rate of presynaptic EC input neuron j , ν_i the firing rate
 748 of postsynaptic DGC i , η the learning rate, θ marks the transition from LTD to

749 LTP, and the relative strength α , γ of LTP and LTD depend on θ via $\alpha = \frac{\alpha_0}{\theta^3} > 0$
750 and $\gamma = \gamma_0 - \theta > 0$. The values of the parameters α_0 , γ_0 , β , and θ are given in Ta-
751 ble 1 (Biologically-plausible network). The weights are hard-bounded from below
752 at 0, i.e. if equation (6) leads to a new weight smaller than zero, w_{ij} is set to zero.
753 The first two terms of equation (6) are a variation of the BCM rule (Bienenstock
754 et al., 1982). The third term implements heterosynaptic plasticity (Chistiakova
755 et al., 2014; Zenke and Gerstner, 2017). Because the first two terms of the plas-
756 ticity rule are Hebbian and proportional to the presynaptic activity x_j , the active
757 DGCs ($\nu_i > \theta$) update their feedforward weights in direction of the input pattern
758 \vec{x} . Moreover, all weights onto neuron i are downregulated heterosynaptically by
759 an amount that increases supra-linearly with the postsynaptic rate ν_i . Similar to
760 learning in a competitive network (Kohonen, 1989; Hertz et al., 1991), the vector
761 of feedforward weights onto active DGCs will move towards the center of mass of
762 the cluster of patterns they are selective for, as we will discuss now.

763 For a given input pattern \vec{x}^μ , there are three fixed points for the postsynaptic
764 firing rate: $\nu_i = 0$, $\nu_i = \theta$, and $\nu_i = \hat{\nu}_i$ (the negative root is omitted, because $\nu_i \geq 0$
765 due to equation (2)). For $\nu_i < \theta$, there is LTD, so the weights move toward zero:
766 $w_{ij} \rightarrow 0$, while for $\nu_i > \theta$, there is LTP, so the weights move toward $w_{ij} \rightarrow \frac{\gamma x_j^\mu}{\beta \nu_i^2}$
767 (Fig. 1c). The value of $\hat{\nu}_i$ is defined implicitly by the network equations (2)-(5). If
768 a pattern \vec{x}^μ is presented only for a short time these fixed points are not reached
769 during a single pattern presentation.

770 **Winners, losers, and quasi-orthogonal inputs**

771 We define the winners as the DGCs which become strongly active ($\nu_i > \theta$) during
772 presentation of an input pattern. Since the input patterns are normalized to have
773 an L2-norm of 1 ($\|\vec{x}^\mu\| = 1$ by construction), and the L2-norm of the feedforward
774 weight vectors is bounded (see Section Direction and length of the weight vector),
775 the winning units are the ones whose weight vectors \vec{w}_i (row of the feedforward
776 connectivity matrix) align best with the current input pattern \vec{x}^μ . Furthermore,
777 we say that an input pattern \vec{x}^μ is “quasi-orthogonal” to a weight vector \vec{w}_i if
778 $I_i = \sum_{j=1}^{N_{EC}} w_{ij} x_j + \sum_{k=1}^{N_I} w_{ik}^{EI} \nu_k^I < b_i$. If an input pattern \vec{x}^μ is quasi-orthogonal
779 to a weight vector \vec{w}_i , then neuron i does not fire in response to \vec{x}^μ . Note that
780 for a case without inhibitory neurons and with $b_i \rightarrow 0$, we recover the standard
781 orthogonality condition.

782 **Direction and length of the weight vector**

783 Let us denote the ensemble of patterns for which neuron i is a winner by C_i and
784 call this the set of winning patterns ($C_i = \{\mu | \nu_i > \theta\}$). Suppose that neuron i

785 is quasi-orthogonal to all other patterns, so that for all $\mu \notin C_i$ we have $\nu_i = 0$.
 786 Then the feedforward weight vector of neuron i converges in expectation to:

$$\vec{w}_i = \frac{\gamma \langle G_1(\nu_i) \vec{x} \rangle_{\mu \in C_i}}{\beta \langle G_2(\nu_i) \rangle_{\mu \in C_i}} \quad (7)$$

787 where $G_1(\nu_i) = (\nu_i - \theta)\nu_i$ and $G_2(\nu_i) = (\nu_i - \theta)\nu_i^3$. Hence \vec{w}_i is a weighted average
 788 over all winning patterns.

The squared length of the feedforward weight vector can be computed by multiplying equation (7) with \vec{w}_i :

$$\|\vec{w}_i\|^2 = \vec{w}_i \cdot \vec{w}_i = \frac{\gamma \langle G_1(\nu_i) (\vec{w}_i \cdot \vec{x}) \rangle_{\mu \in C_i}}{\beta \langle G_2(\nu_i) \rangle_{\mu \in C_i}} \quad (8)$$

789 Since input patterns have length one, the scalar product on the right-hand side
 790 can be rewritten as $\vec{w}_i \cdot \vec{x} = \|\vec{w}_i\| \cos(\alpha)$ where α is the angle between the weight
 791 vector and pattern \vec{x} . Division by $\|\vec{w}_i\|$ yields the L2-norm of the feedforward
 792 weight vector:

$$\|\vec{w}_i\| = \frac{\gamma \langle G_1(\nu_i) \cos(\alpha) \rangle_{\mu \in C_i}}{\beta \langle G_2(\nu_i) \rangle_{\mu \in C_i}} \quad (9)$$

793 where the averages run, as before, over all winning patterns.

794 Let us now derive bounds for $\|\vec{w}_i\|$. First, since $\cos(\alpha) \leq 1$ we have
 795 $\langle G_1(\nu_i) \cos(\alpha) \rangle_{\mu \in C_i} \leq \langle G_1(\nu_i) \rangle_{\mu \in C_i}$. Second, since for all winning patterns $\nu_i > \theta$,
 796 where θ is the LTP threshold, we have $\langle G_2(\nu_i) \rangle_{\mu \in C_i} \geq \langle (\nu_i - \theta) \nu_i \rangle_{\mu \in C_i} \theta^2$. Thus the
 797 length of the weight vector is finite and bounded by:

$$\|\vec{w}_i\| \leq \frac{\gamma \langle G_1(\nu_i) \rangle_{\mu \in C_i}}{\beta \langle G_2(\nu_i) \rangle_{\mu \in C_i}} \leq \frac{\gamma}{\beta \theta^2} \quad (10)$$

798 It is possible to make the second bound tighter if we find the winning pattern
 799 with the smallest firing rate ν_{\min} such that $\nu_i \geq \nu_{\min} \forall i \in C_i$:

$$\|\vec{w}_i\| \leq \frac{\gamma}{\beta (\nu_{\min})^2} \quad (11)$$

800 The bound is reached if neuron i is winner for a single input pattern.

We can also derive a lower bound. For a pattern $\mu \in C_i$, let us write the firing rate of neuron i as $\nu_i(\mu) = \bar{\nu}_i + \Delta\nu_i(\mu)$ where $\bar{\nu}_i$ is the mean firing rate of neuron i averaged across all winning patterns and $\langle \Delta\nu_i \rangle_{\mu \in C_i} = 0$. We assume that the absolute size of $\Delta\nu_i$ is small, i.e., $\langle (\Delta\nu_i)^2 \rangle_{\mu \in C_i} \ll (\bar{\nu}_i)^2$. Linearization of equation (9) around $\bar{\nu}_i$ yields:

$$\|\vec{w}_i\| = \frac{\gamma}{\beta} \frac{G_1(\bar{\nu}_i)}{G_2(\bar{\nu}_i)} \langle \cos(\alpha) \rangle_{\mu \in C_i} + \frac{\gamma}{\beta} \frac{G_1'(\bar{\nu}_i)}{G_2(\bar{\nu}_i)} \langle \cos(\alpha) \Delta\nu_i \rangle_{\mu \in C_i} \quad (12)$$

801 Elementary geometric arguments for a neuron model with monotonically in-
802 creasing frequency-current curve yield that the value of $\langle \cos(\alpha) \Delta \nu_i \rangle_{\mu \in C_i}$ is positive
803 (or zero), because an increase in the angle α lowers both the cosine and the firing
804 rate, giving rise to a positive correlation. Since we are interested in a lower bound,
805 we can therefore drop the term proportional to G'_1 and evaluate the ratio G_1/G_2
806 to find:

$$\|\vec{w}_i\| \geq \frac{\gamma}{\beta} \frac{1}{(\bar{\nu}_i)^2} \langle \cos(\alpha) \rangle_{\mu \in C_i} \geq \frac{\gamma}{\beta} \frac{1}{(\nu_{\max})^2} \cos(\hat{\alpha}) \quad (13)$$

807 where ν_{\max} is the maximal firing rate of a DGC and $\hat{\alpha} = \max_{\mu \in C_i} \{\alpha\}$ is the angle
808 of the winning pattern that has the largest angle with the weight vector. The first
809 bound is tight and is reached if neuron i is winner for only two patterns.

810 To summarize we find that the length of the weight vector remains bounded in
811 a narrow range. Hence, for a reasonable distribution of input patterns and weight
812 vectors, the value of $\|\vec{w}_i\|$ is similar for different neurons i , so that the weight
813 vector will have, after convergence, similar lengths for all DGCs that are winners
814 for at least one pattern. In our simulations with the MNIST data set, we find that
815 the length of feedforward weight vectors lies in the range between 9.3 and 11.1
816 across all responsive neurons with a mean value close to 10; cf. Fig. 2e.

817 Early maturation phase

818 During the early phase of maturation, the GABAergic input onto a newborn
819 DGC with index l has an excitatory effect. In the model, it is implemented as
820 follows: $w_{lk}^{EI} = -w_{EI} > 0$ with probability p_{EI} for any interneuron k and $w_{lk}^{EI} = 0$
821 otherwise (no connection). Since newborn cells do not project yet onto inhibitory
822 neurons (Temprana et al., 2015), we have $w_{kl}^{IE} = 0 \forall l$. Newborn DGCs are known
823 to have enhanced excitability (Schmidt-Hieber et al., 2004; Li et al., 2017), so
824 their threshold is kept at $b_l = 0 \forall l$. Because the newborn model DGCs receive
825 lateral excitation via interneurons and their thresholds are zero during the early
826 phase of maturation, the lateral excitatory GABAergic input is always sufficient
827 to activate them. Hence, if the firing rate of a newborn DGC exceeds the LTP
828 threshold θ , the feedforward weights grow towards the presented input pattern,
829 cf. equation (6).

830 Presentation of all patterns of the data set once (1 epoch) is sufficient to reach
831 convergence of the feedforward weights onto newborn DGCs. We define the end
832 of the first epoch as the end of the early phase, i.e., simulation of one epoch of
833 the model corresponds to about three weeks of biological time.

834 Late maturation phase

835 During the late phase of maturation (starting at about 3 weeks (Ge et al., 2006)),
836 the GABAergic input onto newborn DGCs switches from excitatory to inhibitory.
837 In terms of our model, it means that all existing w_{ik}^{EI} connections switch their
838 sign to $w_{EI} < 0$. Furthermore, since newborn DGCs develop lateral connections
839 to inhibitory neurons in the late maturation phase (Temprana et al., 2015), we
840 set $w_{kl}^{IE} = w_{IE}$ with probability p_{IE} , and $w_{kl}^{IE} = 0$ otherwise. The thresholds of
841 newborn DGCs are updated after presentation of pattern μ at time $n \cdot T$ ($b_l^{(n)} =$
842 $b_l^{(n-1)} + \Delta b_l$) according to $\Delta b_l = \eta_b (\nu_l - \nu_0)$, where ν_0 is a reference rate and η_b
843 a learning rate, to mimic the decrease of excitability as newborn DGCs mature
844 (Table 1, Biologically-plausible network). Therefore the distribution of firing rates
845 of newborn DGCs is shifted to the left (towards lower firing rates) at the end of the
846 late phase of maturation compared to the early phase of maturation (Fig. 2c,d). A
847 sufficient condition for a newborn DGC to win the competition upon presentation
848 of patterns of the novel cluster is that the scalar product between a pattern of
849 the novel cluster and the feedforward weight vector onto the newborn DGC is
850 larger than the scalar product between the pattern of the novel cluster and the
851 feedforward weight vector onto any of the mature DGCs. Analogous to the early
852 phase of maturation, presentation of all patterns of the data set once (1 epoch)
853 is sufficient to reach convergence of the feedforward weights onto newborn DGCs.
854 We therefore consider that the late phase of maturation has been finished after
855 one epoch.

856 Input patterns

857 Two different sets of input patterns are used. Both data sets have a number K
858 of clusters and several thousands of patterns per cluster. As a first data set, we
859 use the MNIST 12x12 patterns (LeCun et al., 1998) ($N_{EC} = 144$), normalized
860 such that the L2-norm of each pattern is equal to 1. The training set contains
861 approximately 6000 patterns per digit, while the testing set contains about 1000
862 patterns per digit (Fig. 1d).

863 As a second data set, we use hand-made artificial patterns designed such that
864 the distance between the centers of any two clusters, or in other words their
865 pairwise similarity, is the same. All clusters lie on the positive quadrant of the
866 surface of a hypersphere of dimension $N_{EC} - 1$. The cluster centers are Walsh

867 patterns shifted along the diagonal (Fig. 5b):

$$\begin{aligned}
 \vec{P}^1 &= \frac{1}{c_0} (1 + \xi, 1 - \xi, 1 + \xi, 1 - \xi, \dots, 1 + \xi, 1 - \xi, 1 + \xi, 1 - \xi) \\
 \vec{P}^2 &= \frac{1}{c_0} (1 + \xi, 1 + \xi, 1 - \xi, 1 - \xi, \dots, 1 + \xi, 1 + \xi, 1 - \xi, 1 - \xi) \\
 &\dots \\
 \vec{P}^K &= \frac{1}{c_0} (1 + \xi, 1 + \xi, 1 + \xi, 1 + \xi, \dots, 1 - \xi, 1 - \xi, 1 - \xi, 1 - \xi)
 \end{aligned} \tag{14}$$

868 with $|\xi| < 1$ a parameter that determines the spacing between clusters. c_0 is
 869 a normalization factor to ensure that the center of mass of all clusters has an
 870 L2-norm of 1:

$$c_0 = \sqrt{N_{EC}(1 + \xi^2)}. \tag{15}$$

871 The number of input neurons N_{EC} is $N_{EC} = 2^K$. The scalar product, and hence
 872 the angle Ω , between the center of mass of any pair of clusters k and l ($k \neq l$) is
 873 a function of ξ (Fig. 5a):

$$\vec{P}^k \cdot \vec{P}^l = \frac{1}{1 + \xi^2} = \cos(\Omega) \tag{16}$$

874 We define the pairwise similarity s of two clusters as: $s = 1 - \xi$. Highly similar
 875 clusters have a large s due to the small distance between their centers (hence a
 876 small ξ).

877 To make the artificial data set comparable to the MNIST 12x12 data set, we
 878 choose $K = 7$, so $N_{EC} = 128$, and we generate 6000 noisy patterns per cluster for
 879 the training set and 1000 other noisy patterns per cluster for the testing set. Since
 880 our noisy high-dimensional input patterns have to be symmetrically distributed
 881 around the centers of mass \vec{P}^k , yet lie on the hypersphere, we have to use an
 882 appropriate sampling method. The patterns $\vec{x}^{\mu(k)}$ of a given cluster k with center
 883 of mass \vec{P}^k are thus sampled from a Von Mises-Fisher distribution (Mardia and
 884 Jupp, 2009):

$$\vec{x}^{\mu(k)} \sim \left(\sqrt{1 - a^2} \right) \vec{\zeta} + a\vec{P}^k \tag{17}$$

885 with $\vec{\zeta}$ an L2-normalized vector taken in the space orthogonal to \vec{P}^k . The vector $\vec{\zeta}$
 886 is obtained by performing the singular-value decomposition of \vec{P}^k ($U\Sigma V^* = \vec{P}^k$),
 887 and multiplying the matrix U (after removing its first column), which corresponds
 888 to the left-singular vectors in the orthogonal space to \vec{P}^k , with a vector whose
 889 elements are drawn from the standard normal distribution. Then the L2-norm of
 890 the obtained pattern is set to 1, so that it lies on the surface of the hypersphere.
 891 A rejection sampling scheme is used to obtain a (Mardia and Jupp, 2009). The
 892 sample a is kept if $\kappa a + (N_{EC} - 1)\ln(1 - \psi a) - c \geq \ln(u)$, with κ a concentration
 893 parameter, $\psi = \frac{1-b}{1+b}$, $c = \kappa\psi + (N_{EC} - 1)\ln(1 - \psi^2)$, u drawn from a uniform

894 distribution $u \sim U[0, 1]$, $a = \frac{1-(1+b)z}{1-(1-b)z}$, $b = \frac{N_{EC}-1}{\sqrt{4\kappa^2+(N_{EC}-1)^2+2\kappa}}$, and z drawn from a
 895 beta distribution $z \sim \mathcal{B}e(\frac{N_{EC}-1}{2}, \frac{N_{EC}-1}{2})$.

896 The concentration parameter κ characterizes the spread of the distribution
 897 around the center \vec{P}^k . In the limit where $\kappa \rightarrow 0$, sampling from the Von Mises-
 898 Fisher distribution becomes equivalent to sampling uniformly on the surface of the
 899 hypersphere, so the clusters become highly overlapping. In dimension $N_{EC} = 128$,
 900 if $\kappa > 10^3$ the probability of overlap between clusters is negligible. We use a value
 901 $\kappa = 10^4$.

902 Classification performance (readout network)

903 It has been observed that classification performance based on DGC population
 904 activity is a good proxy for behavioral discrimination (Woods et al., 2020). Hence,
 905 to evaluate whether the newborn DGCs contribute to the function of the dentate
 906 gyrus network, we study classification performance. Once the feedforward weights
 907 have been adjusted upon presentation of many input patterns from the training
 908 set (Section Plasticity rule), we keep them fixed and determine classification on
 909 the test set using artificial readout units (RO).

910 To do so, the readout weights (w_{ki}^{RO} from model DGC i to readout unit k) are
 911 initialized at random values drawn from a uniform distribution: $w_{ki}^{RO} \sim \sigma\mathcal{U}(0, 1)$,
 912 with $\sigma = 0.1$. The number of readout units, N_{RO} , corresponds to the number of
 913 learned classes. To adjust the readout weights, all patterns of the training data
 914 set that belong to the learned classes are presented one after the other. For each
 915 pattern \vec{x}^μ , we let the firing rate of the DGCs converge (values at convergence:
 916 ν_i^μ). The activity of a readout unit k is given by:

$$\nu_k^{RO,\mu} = g\left(I_k^{RO,\mu}\right) = g\left(\sum_{i=1}^{N_{DGC}} w_{ki}^{RO} \nu_i^\mu\right) \quad (18)$$

As we aim to assess the performance of the network of DGCs, the readout weights are adjusted by an artificial supervised learning rule. The loss function, which corresponds to the difference between the activity of the readout units and a one-hot representation of the corresponding pattern label (Hertz et al., 1991),

$$L(W^{RO}) = \frac{1}{2} \sum_{k=1}^{N_{RO}} (L_k^\mu - \nu_k^{RO,\mu})^2 \quad (19)$$

917 with L_k^μ the element k of a one-hot representation of the correct label of pattern
 918 \vec{x}^μ , is minimized by stochastic gradient descent:

$$\Delta w_{ki}^{RO,\mu} = \eta(L_k^\mu - \nu_k^{RO,\mu})g'\left(I_k^{RO,\mu}\right)\nu_i^\mu. \quad (20)$$

919 The readout units have a rectified hyperbolic tangent frequency-current curve:
920 $g(x) = \tanh(2[x]_+)$, whose derivative is: $g'(x) = 2(1 - (\tanh(2[x]_+))^2)$. We learn
921 the weights of the readout units over 100 epochs of presentations of all training
922 patterns with $\eta = 0.01$, which is sufficient to reach convergence.

923 Thereafter, the readout weights are fixed. Each test set pattern belonging to
924 one of the learned classes is presented once, and the firing rates of the DGCs are
925 let to converge. Finally, the activity of the readout units $\nu_k^{RO,\mu}$ is computed and
926 compared to the correct label L_k^μ of the presented pattern. If the readout unit with
927 the highest activity value is the one that represents the class of the presented input
928 pattern, the pattern is said to be correctly classified. Classification performance
929 is given by the number of correctly classified patterns divided by the total number
930 of test patterns of the learned classes.

931 Control cases

932 In our standard setting, patterns from a third digit are presented to a network
933 that has previously only seen patterns from two digits. The question is whether
934 neurogenesis helps when adding the third digit. We use several control cases to
935 compare with the neurogenesis case. In the first control case, all three digits are
936 learned in parallel (Fig. 3a, control 1). In the two other control cases, we either
937 keep all feedforward connections towards the DGCs plastic (Fig. 3c, control 3),
938 or fix the feedforward connections for all selective DGCs but keep unselective
939 neurons plastic (as in the neurogenesis case) (Fig. 3b, control 2). However, in
940 both instances, the DGCs do not mature in the two-step process induced by the
941 GABA-switch that is part of our model of neurogenesis.

942 Pretraining with two digits

943 As we are interested by neurogenesis at the adult stage, we pretrain the network
944 with patterns from two digits, such that it already stores some memories before
945 neurogenesis takes place. To do so, we randomly initialize the weights from EC
946 neurons to DGCs: they are drawn from a uniform distribution ($w_{ij} \sim U[0, 1]$).
947 The L2-norm of the feedforward weight vector onto each DGC is then normal-
948 ized to 1, to ensure fair competition between DGCs during learning. Then we
949 present all patterns from digits 3 and 4 in random order, as many times as needed
950 for convergence of the weights. During each pattern presentation the firing rates
951 of the DGCs are computed (Section Network architecture and neuronal dynam-
952 ics) and their feedforward weights are updated according to our plasticity rule
953 (Section Plasticity rule). We find that we need approximately 40 epochs for con-
954 vergence of the weights, and use 80 epochs to make sure that all weights are stable.

955 At the end of pretraining, our network is considered to correspond to an adult
956 stage, because some DGCs are selective for prototypes of the pretrained digits
957 (Fig. 1e).

958 Projection on pairwise discriminatory axes

959 To assess how separability of the DGC activation patterns develops during the
960 late phase of maturation of newborn DGCs, we project the population activity
961 onto axes which are optimized for pairwise discrimination (patterns from digit 3
962 versus patterns from digit 5, 4 versus 5, and 3 vs 4). Those axes are determined
963 using Fisher linear discriminant analysis (LDA), as explained below.

964 We determine the vector of DGC firing rates, \vec{v} , at the end of the late phase of
965 maturation of newborn DGCs upon presentation of each pattern, \vec{x} , from digits
966 3, 4 and 5 of the training MNIST dataset. The mean activity in response to all
967 training patterns μ from digit m , $\vec{\mu}_m = \frac{1}{N_m} \sum_{\mu \in m} \vec{v}^\mu$, is computed for each of
968 the three digits (N_m is the number of training patterns of digit m). The pairwise
969 Fisher linear discriminant is defined as the linear function $\vec{w}^T \vec{v}$ that maximizes the
970 distance between the means of the projected activity in response to two digits (eg.
971 m and n), while normalizing for within-digit variability. The objective function
972 to maximize is thus given as:

$$J(w) = \frac{w^T S_B w}{w^T S_W w} \quad (21)$$

973 with $S_B = (\vec{\mu}_m - \vec{\mu}_n)(\vec{\mu}_m - \vec{\mu}_n)^T$ the between-digit scatter matrix, and $S_W =$
974 $\Sigma_m + \Sigma_n$ the within-digit scatter matrix (Σ_m is the covariance matrix of the DGC
975 activity in response to pattern of digit m , and Σ_n is the covariance matrix of
976 the DGC activity in response to pattern of digit n). It can be shown that the
977 direction of the optimal discriminatory axis between digit m and n is given by the
978 eigenvector of $S_W^{-1} S_B$ with the corresponding largest eigenvalue.

979 We arbitrarily set "axis 1" as the optimal discriminatory axis between digit
980 3 and digit 5, "axis 2" as the optimal discriminatory axis between digit 4 and
981 digit 5, and "axis 3" as the optimal discriminatory axis between digit 3 and digit
982 4. For each of the three discriminatory axes, we define its origin (ie. projection
983 value of 0) as the location of the average projection of all training patterns of the
984 three digits on the corresponding axis. Fig. 4 represents the projections of DGC
985 activity upon presentation of testing patterns at the end of the early and late
986 phase of maturation of newborn DGCs onto the above-defined axes.

987 Statistics

988 In the main text, we present a representative example with three digits from the
989 MNIST data set (3, 4 and 5). It is selected from a set of ten random combinations
990 of three different digits. For each combination, one network is pretrained with
991 two digits for 80 epochs. Then the third digit is added and neurogenesis takes
992 place (one epoch of early phase of maturation, and one epoch of late phase of
993 maturation). Furthermore another network is pretrained directly with the three
994 digits for 80 epochs. Classification performance is reported for all combinations
995 (Suppl. Table S1).

996 Simplified rate network

997 We use a toy network and the artificial data set to determine if our theory of
998 integration of newborn DGCs can explain why adult dentate gyrus neurogenesis
999 helps for the discrimination of similar, but not for distinct patterns.

1000 The rate network described above is simplified as follows. We use K dentate
1001 granule cells for K clusters. Their firing rate ν_i is given by:

$$\tau_m \frac{d\nu_i}{dt} = -\nu_i + \mathcal{H}(I_i - b_i) \quad (22)$$

1002 where \mathcal{H} is the Heaviside step function. As before, b_i is the threshold, and I_i the
1003 total input towards neuron i :

$$I_i = \sum_{j=1}^{N_{EC}} w_{ij} x_j + \sum_{k \neq j}^{N_{DGC}} w_{rec} \nu_k \quad (23)$$

1004 with x_j the input of presynaptic EC neuron j , w_{ij} the feedforward weight between
1005 EC neuron j and DGC i , and ν_k the firing rate of DGC k . Inhibitory neurons are
1006 modeled implicitly: each DGC directly connects to all other DGCs via inhibitory
1007 recurrent connections of value $w_{rec} < 0$. During presentation of pattern \vec{x}^μ , the
1008 firing rates of the DGCs evolve according to equation (22). After convergence, the
1009 feedforward weights are updated: $w_{ij}^{(\mu)} = w_{ij}^{(\mu-1)} + \Delta w_{ij}$. The synaptic plasticity
1010 rule is the same as before, see equation (6), but with the parameters reported
1011 in Table 1(Simple network). They are different from those of the biologically-
1012 plausible network because we now aim for a single winning neuron for each cluster.
1013 Note that for an LTP threshold $\theta < 1$ all active DGCs update their feedforward
1014 weights, because of the Heaviside function for the firing rate (equation (22)).

1015 Assuming a single winner i^* for each pattern presentation, the input (equa-
1016 tion (23)) to the winner is:

$$I_{i^*} = \vec{w}_{i^*} \cdot \vec{x}, \quad (24)$$

1017 while the input to the losers is:

$$I_i = \vec{w}_i \cdot \vec{x} + w_{\text{rec}}. \quad (25)$$

1018 Therefore, two conditions need to be satisfied for a solution with a single winner:

$$\vec{w}_{i^*} \cdot \vec{x} > b_i \quad (26)$$

1019 for the winner to actually be active, and:

$$\vec{w}_i \cdot \vec{x} + w_{\text{rec}} < b_i \quad (27)$$

1020 to prevent non-winners to become active. The value of b_i in the model is lower in
 1021 the early phase than in the late phase of maturation to mimic enhanced excitabil-
 1022 ity (Schmidt-Hieber et al., 2004; Li et al., 2017).

1023 **Similar versus distinct patterns with the artificial data set**

1024 Using the artificial data set with $|\xi| < 1$ (equation (14)), the scalar product
 1025 between the centers of mass of two different clusters, given by equation (16),
 1026 satisfies: $0.5 \leq \frac{1}{1+\xi^2} \leq 1$. This corresponds to $0^\circ \leq \Omega \leq \Omega_{\text{max}} = 60^\circ$.

1027 After stimulation with a pattern \vec{x} , it takes some time before the firing rates
 1028 of the DGCs converge. We call two patterns “similar” if they activate, at least
 1029 initially, the same output unit, while we consider two patterns as “distinct” if
 1030 they do not activate the same output unit, not even initially. We now show that,
 1031 with a large concentration parameter κ , patterns of different clusters are similar
 1032 if $\xi < \sqrt{\frac{\|\vec{w}_i\|}{b_i} - 1}$ and distinct if $\xi > \sqrt{\frac{\|\vec{w}_i\|}{b_i} - 1}$.

1033 We first consider a DGC i whose feedforward weight vector has converged
 1034 towards the center of mass of cluster k . If an input pattern $\vec{x}^{\mu(k)}$ from cluster k
 1035 is presented, it will receive the following initial input:

$$I_i = \vec{w}_i \cdot \vec{x}^{\mu(k)} = \|\vec{w}_i\| \cdot \|\vec{x}^{\mu(k)}\| \cdot \cos(\vartheta_{kk}) = \|\vec{w}_i\| \cdot \cos(\vartheta_{kk}) \quad (28)$$

1036 where ϑ_{kk} is the angle between the pattern $\vec{x}^{\mu(k)}$ and the center of mass \vec{P}^k of
 1037 the cluster to which it belongs. The larger the concentration parameter κ for the
 1038 generation of the artificial data set, the smaller the dispersion of the clusters, and
 1039 thus the larger $\cos(\vartheta_{kk})$. If instead, an input pattern from cluster l is presented,
 1040 that same DGC will receive a lower initial input:

$$I_i = \vec{w}_i \cdot \vec{x}^{\mu(l)} = \|\vec{w}_i\| \cdot \|\vec{x}^{\mu(l)}\| \cdot \cos(\vartheta_{kl}) \approx \frac{\|\vec{w}_i\|}{1 + \xi^2} \quad (29)$$

1041 The approximation holds for a small dispersion of the clusters (large concentra-
 1042 tion parameter κ). We note that there is no subtraction of the recurrent input

1043 yet, because output units are initialized with zero firing rate before each pattern
 1044 presentation. By definition, similar patterns stimulate (initially) the same DGCs.
 1045 A DGC can be active for two clusters only if its threshold is:

$$b_i < \frac{\|\vec{w}_i\|}{1 + \xi^2} \quad (30)$$

1046 Therefore, with a high concentration parameter κ , patterns of different clusters
 1047 are similar if $\xi < \sqrt{\frac{\|\vec{w}_i\|}{b_i} - 1}$, while patterns of different clusters are distinct if
 1048 $\xi > \sqrt{\frac{\|\vec{w}_i\|}{b_i} - 1}$.

1049 Parameter choice

1050 The upper bound of the expected L2-norm of the feedforward weight vector to-
 1051 wards the DGCs at convergence can be computed, see equation (11). With the
 1052 parameters in Table 1(Simple network), the value is $\|\vec{w}_i\| \leq 1.5$. Moreover, the
 1053 input patterns for each cluster are highly concentrated, hence their angle with the
 1054 center of mass of the cluster they belong to is close to 0, so we have $\|\vec{w}_i\| \approx 1.5$.
 1055 Therefore, at convergence, a DGC selective for a given cluster k receives an input
 1056 $I_{i^*} = \vec{w}_{i^*} \cdot \vec{x}^{\mu(k)} \approx 1.5$ upon presentation of input patterns $\vec{x}^{\mu(k)}$ belonging to cluster
 1057 k . We choose $b_i = 1.2$ to satisfy equation (26). Given b_i the threshold value ξ_{thresh}
 1058 for which two clusters are similar (and above which two clusters are distinct) can
 1059 be determined by equation (30) : $\xi_{\text{thresh}} = 0.5$. We created a handmade data set
 1060 with $\xi = 0.2$ for the case of similar clusters (therefore with similarity $s = 0.8$),
 1061 and a handmade data set with $\xi = 0.8$ for the distinct case (hence with similarity
 1062 $s = 0.2$).

1063 Let us suppose that the weights of DGC i have converged and made this cell
 1064 respond to patterns of cluster i . If another DGC k of the network is selective
 1065 for cluster k , cell i gets the input $I_i = \vec{w}_i \cdot \vec{x}^{\mu(k)} + w_{\text{rec}} \approx \frac{1.5}{1+\xi^2} + w_{\text{rec}}$ upon
 1066 presentation of input patterns $\vec{x}^{\mu(k)}$ belonging to cluster $k \neq i$. Hence, to satisfy
 1067 equation (27), we need $w_{\text{rec}} < b_i - \max_{\xi} \left(\frac{1.5}{1+\xi^2} \right) \approx -0.24$. We set $w_{\text{rec}} = -1.2$.

1068 Furthermore, a newborn DGC is born with a null feedforward weight vector so
 1069 that at birth, its input consists only of the indirect excitatory input from mature
 1070 DGCs which vanishes if all DGCs are quiescent and takes a value $I_i = -w_{\text{rec}} > 0$
 1071 if a mature DGC responds to the input. For the feedforward weight vector to grow,
 1072 the newborn cell i needs to be active. This could be achieved through spontaneous
 1073 activity which could be implemented by setting the intrinsic firing threshold at
 1074 birth to a value $b_{\text{birth}} < 0$. In this case a difference between similar and distinct
 1075 patterns is not expected. Alternatively, activity of newborn cells can be achieved
 1076 in the absence of spontaneous activity under the condition $-w_{\text{rec}} > b_{\text{birth}}$. For the

1077 simulations with the toy model, we set $b_{\text{birth}} = 0.9$ which leads to weight growth
1078 in newborn cells for similar, but not distinct patterns.

1079 Neurogenesis with the artificial data set

1080 To save computation time, we initialize the feedforward weight vectors of two
1081 mature DGCs at two training patterns randomly chosen from the first two clusters,
1082 normalized such that they have an L2-norm of 1.5. We then present patterns from
1083 clusters 1 and 2, and let the feedforward weights evolve according to equation (6)
1084 until they reach convergence.

1085 We thereafter fix the feedforward weights onto the two mature cells, and in-
1086 troduce a novel cluster of patterns as well as a newborn DGC in the network. The
1087 sequence of presentation of patterns from the three clusters (a novel one and two
1088 pretrained ones) is random. The newborn DGC is born with a null feedforward
1089 weight vector, and its maturation follows the same rules as before (plastic feedfor-
1090 ward weights). In the early phase, GABAergic input has an excitatory effect (Ge
1091 et al., 2006) and the newborn DGC does not inhibit the mature DGCs (Temprana
1092 et al., 2015). This is modeled by setting $w_{\text{rec}}^{NM} = -w_{\text{rec}}$ for the connections from
1093 mature to newborn DGC, and $w_{\text{rec}}^{MN} = 0$ for the connections from newborn to
1094 mature DGCs. The threshold of the newborn DGC starts at $b_{\text{birth}} = 0.9$ at birth,
1095 mimicking enhanced excitability (Schmidt-Hieber et al., 2004; Li et al., 2017),
1096 and increases linearly up to 1.2 (same threshold as that of mature DGCs) over
1097 12000 pattern presentations, reflecting loss of excitability with maturation. The
1098 exact time window is not critical. In the late phase of maturation of the newborn
1099 DGC, GABAergic input switches to inhibitory (Ge et al., 2006), and the newborn
1100 DGC recruits feedback inhibition onto mature DGCs (Temprana et al., 2015).
1101 It is modeled by switching the sign of the connection from mature to newborn
1102 DGC: $w_{\text{rec}}^{NM} = w_{\text{rec}}$, and establishing connections from newborn to mature DGCs:
1103 $w_{\text{rec}}^{MN} = w_{\text{rec}}$. Each of the 6000 patterns is presented once during the early phase
1104 of maturation, and once during the late phase of maturation.

1105 The above paradigm is run separately for each of the two handmade data
1106 sets: the one where clusters are similar ($s = 0.8$), and the one where clusters are
1107 distinct ($s = 0.2$).

1108 Acknowledgments

1109 This research was supported by the Swiss National Science Foundation (no.
1110 200020_184615) and by the European Union Horizon 2020 Framework Program
1111 under grant agreement no. 785907 (HumanBrain Project, SGA2).

1112 **Authors contributions**

1113 O.G. developed the model and carried out the simulations. W.G. participated in
1114 discussions and helped designing the project. O.G. and W.G. wrote and validated
1115 the manuscript.

1116 **Declaration of interests**

1117 The authors declare no competing interests.

1118 **References**

- 1119 Acsády, L., Kamondi, A., Sík, A., Freund, T., and Buzsáki, G. (1998). GABAergic
1120 cells are the major postsynaptic targets of mossy fibers in the rat hippocampus.
1121 *Journal of neuroscience*, 18, 3386–3403.
- 1122 Aimone, J. B., Deng, W., and Gage, F. H. (2011). Resolving new memories: a
1123 critical look at the dentate gyrus, adult neurogenesis, and pattern separation.
1124 *Neuron*, 70, 589–596.
- 1125 Aimone, J. B., Wiles, J., and Gage, F. H. (2009). Computational influence of
1126 adult neurogenesis on memory encoding. *Neuron*, 61, 187–202.
- 1127 Albus, J. (1971). A theory of cerebellar function. *J. Mathematical Biosciences*,
1128 10, 25–61.
- 1129 Alvarez, D. D., Giacomini, D., Yang, S. M., Trincherro, M. F., Temprana, S. G.,
1130 Büttner, K. A., Beltramone, N., and Schinder, A. F. (2016). A disynaptic feed-
1131 back network activated by experience promotes the integration of new granule
1132 cells. *Science*, 354, 459–465.
- 1133 Amaral, D. G., Scharfman, H. E., and Lavenex, P. (2007). The dentate gyrus: fun-
1134 damental neuroanatomical organization (dentate gyrus for dummies). *Progress*
1135 *in brain research*, 163, 3–22.
- 1136 Andersen, P., Morris, R., Amaral, D., Bliss, T., and O’Keefe, J. eds. (2007). *The*
1137 *hippocampus book*. (Oxford university press).
- 1138 Appleby, P. A. and Wiskott, L. (2009). Additive neurogenesis as a strategy for
1139 avoiding interference in a sparsely-coding dentate gyrus. *Network: Computation*
1140 *in Neural Systems*, 20, 137–161.

- 1141 Artola, A., Bröcher, S., and Singer, W. (1990). Different voltage dependent thresh-
1142 olds for inducing long-term depression and long-term potentiation in slices of
1143 rat visual cortex. *Nature*, 347, 69–72.
- 1144 Babadi, B. and Sompolinsky, H. (2014). Sparseness and expansion in sensory
1145 representations. *Neuron*, 83, 1213–1226.
- 1146 Barmashenko, G., Hefft, S., Aertsen, A., Kirschstein, T., and Köhling, R. (2011).
1147 Positive shifts of the GABA_A receptor reversal potential due to altered chloride
1148 homeostasis is widespread after status epilepticus. *Epilepsia*, 52, 1570–1578.
- 1149 Becker, S. (2005). A computational principle for hippocampal learning and neu-
1150 rogenesis. *Hippocampus*, 15, 722–738.
- 1151 Ben-Ari, Y. (2002). Excitatory actions of GABA during development: the nature
1152 of the nurture. *Nature Reviews Neuroscience*, 3, 728–739.
- 1153 Bienenstock, E. L., Cooper, L. N., and Munro, P. W. (1982). Theory for the devel-
1154 opment of neuron selectivity: Orientation specificity and binocular interaction
1155 in visual cortex. *Journal of Neuroscience*, 2, 32–48.
- 1156 Cameron, H. A. and McKay, R. D. (2001). Adult neurogenesis produces a large
1157 pool of new granule cells in the dentate gyrus. *Journal of Comparative Neurol-
1158 ogy*, 435, 406–417.
- 1159 Chambers, R. A. and Conroy, S. K. (2007). Network modeling of adult neuro-
1160 genesis: shifting rates of neuronal turnover optimally gears network learning
1161 according to novelty gradient. *Journal of cognitive neuroscience*, 19, 1–12.
- 1162 Chambers, R. A., Potenza, M. N., Hoffman, R. E., and Miranker, W. (2004).
1163 Simulated apoptosis/neurogenesis regulates learning and memory capabilities
1164 of adaptive neural networks. *Neuropsychopharmacology*, 29, 747–758.
- 1165 Chancey, J. H., Adlaf, E. W., Sapp, M. C., Pugh, P. C., Wadiche, J. I.,
1166 and Overstreet-Wadiche, L. S. (2013). GABA depolarization is required for
1167 experience-dependent synapse unsilencing in adult-born neurons. *Journal of
1168 Neuroscience*, 33, 6614–6622.
- 1169 Chawla, M., Guzowski, J., Ramirez-Amaya, V., Lipa, P., Hoffman, K., Marriott,
1170 L., Worley, P., McNaughton, B., and Barnes, C. A. (2005). Sparse, environmen-
1171 tally selective expression of Arc RNA in the upper blade of the rodent fascia
1172 dentata by brief spatial experience. *Hippocampus*, 15, 579–586.
- 1173 Chistiakova, M., Bannon, N., Bazhenov, M., and Volgushev, M. (2014). Heterosy-
1174 naptic plasticity: Multiple mechanisms and multiple roles. *The Neuroscientist*,
1175 20, 483–498.

- 1176 Clelland, C., Choi, M., Romberg, C., Clemenson, G., Fragniere, A., Tyers, P.,
1177 Jessberger, S., Saksida, L., Barker, R., Gage, F., and Bussey, T. (2009). A
1178 functional role for adult hippocampal neurogenesis in spatial pattern separation.
1179 *Science*, 325, 210–213.
- 1180 Crick, C. and Miranker, W. (2006). Apoptosis, neurogenesis, and information
1181 content in hebbian networks. *Biological cybernetics*, 94, 9–19.
- 1182 Danielson, N. B., Kaifosh, P., Zaremba, J. D., Lovett-Barron, M., Tsai, J., Denny,
1183 C. A., Balough, E. M., Goldberg, A. R., Drew, L. J., Hen, R., Losonczy, A.,
1184 and Kheirbek, M. A. (2016). Distinct contribution of adult-born hippocampal
1185 granule cells to context encoding. *Neuron*, 90, 101–112.
- 1186 Dayer, A. G., Ford, A. A., Cleaver, K. M., Yassaee, M., and Cameron, H. A.
1187 (2003). Short-term and long-term survival of new neurons in the rat dentate
1188 gyrus. *Journal of Comparative Neurology*, 460, 563–572.
- 1189 DeCostanzo, A. J., Fung, C. C. A., and Fukai, T. (2019). Hippocampal neuroge-
1190 nesis reduces the dimensionality of sparsely coded representations to enhance
1191 memory encoding. *Frontiers in computational neuroscience*, 12, 99.
- 1192 Deng, W., Aimone, J. B., and Gage, F. H. (2010). New neurons and new memories:
1193 how does adult hippocampal neurogenesis affect learning and memory? *Nature*
1194 *reviews neuroscience*, 11, 339–350.
- 1195 Deshpande, A., Bergami, M., Ghanem, A., Conzelmann, K.-K., Lepier, A., Götz,
1196 M., and Berninger, B. (2013). Retrograde monosynaptic tracing reveals the
1197 temporal evolution of inputs onto new neurons in the adult dentate gyrus and
1198 olfactory bulb. *Proceedings of the National Academy of Sciences*, 110, 1152–
1199 1161.
- 1200 DeSieno, D. (1988). Adding a conscience to competitive learning. In *IEEE interna-*
1201 *tional conference on neural networks*, vol. 1, pp. 117–124. Institute of Electrical
1202 and Electronics Engineers New York.
- 1203 Du, K.-L. (2010). Clustering: A neural network approach. *Neural networks*, 23,
1204 89–107.
- 1205 Finnegan, R. and Becker, S. (2015). Neurogenesis paradoxically decreases both
1206 pattern separation and memory interference. *Frontiers in systems neuroscience*,
1207 9, 136.
- 1208 Freund, T. and Buzsáki, G. (1996). Interneurons of the hippocampus. *Hippocam-*
1209 *pus*, 6, 347–470.

- 1210 Furukawa, M., Tsukahara, T., Tomita, K., Iwai, H., Sonomura, T., Miyawaki, S.,
1211 and Sato, T. (2017). Neonatal maternal separation delays the GABA excitatory-
1212 to-inhibitory functional switch by inhibiting KCC2 expression. *Biochemical and*
1213 *biophysical research communications*, 493, 1243–1249.
- 1214 Fyhn, M., Hafting, T., Treves, A., Moser, M.-B., and Moser, E. I. (2007). Hip-
1215 pocampal remapping and grid realignment in entorhinal cortex. *Nature*, 446,
1216 190–194.
- 1217 Ganguly, K., Schinder, A. F., Wong, S. T., and Poo, M.-m. (2001). GABA
1218 itself promotes the developmental switch of neuronal GABAergic responses from
1219 excitation to inhibition. *Cell*, 105, 521–532.
- 1220 Ge, S., Goh, E. L., Sailor, K. A., Kitabatake, Y., Ming, G.-l., and Song, H. (2006).
1221 GABA regulates synaptic integration of newly generated neurons in the adult
1222 brain. *Nature*, 439, 589–593.
- 1223 Ge, S., Yang, C.-h., Hsu, K.-s., Ming, G.-l., and Song, H. (2007). A critical period
1224 for enhanced synaptic plasticity in newly generated neurons of the adult brain.
1225 *Neuron*, 54, 559–566.
- 1226 Gilbert, P. E., Kesner, R. P., and Lee, I. (2001). Dissociating hippocampal sub-
1227 regions: A double dissociation between dentate gyrus and CA1. *Hippocampus*,
1228 11, 626–636.
- 1229 Groisman, A. I., Yang, S. M., and Schinder, A. F. (2020). Differential coupling
1230 of adult-born granule cells to parvalbumin and somatostatin interneurons. *Cell*
1231 *reports*, 30, 202–214.
- 1232 Grossberg, S. (1976). Adaptive pattern classification and universal recoding II:
1233 Feedback, expectation, olfaction, illusions. *Biological Cybernetics*, 23, 187–202.
- 1234 Grossberg, S. (1987). *The Adaptive Brain I*. (Elsevier).
- 1235 Heigele, S., Sultan, S., Toni, N., and Bischofberger, J. (2016). Bidirectional
1236 GABAergic control of action potential firing in newborn hippocampal granule
1237 cells. *Nature neuroscience*, 19, 263–270.
- 1238 Henze, D. A., Wittner, L., and Buzsáki, G. (2002). Single granule cells reliably
1239 discharge targets in the hippocampal CA3 network in vivo. *Nature neuroscience*,
1240 5, 790–795.
- 1241 Hertz, J., Krogh, A., and Palmer, R. G. (1991). *Introduction to the Theory of*
1242 *Neural Computation*. (Addison-Wesley).
- 1243 Houser, C. R. (2007). Interneurons of the dentate gyrus: an overview of cell
1244 types, terminal fields and neurochemical identity. *Progress in brain research*,
1245 163, 217–232.

- 1246 Hunsaker, M. R. and Kesner, R. P. (2008). Evaluating the differential roles of the
1247 dorsal dentate gyrus, dorsal CA3, and dorsal CA1 during a temporal ordering
1248 for spatial locations task. *Hippocampus*, 18, 955–964.
- 1249 Jarrard, L. E. (1993). On the role of the hippocampus in learning and memory
1250 in the rat. *Behavioral and neural biology*, 60, 9–26.
- 1251 Jessberger, S., Clark, R. E., Broadbent, N. J., Clemenson, G. D., Consiglio, A.,
1252 Lie, D. C., Squire, L. R., and Gage, F. H. (2009). Dentate gyrus-specific knock-
1253 down of adult neurogenesis impairs spatial and object recognition memory in
1254 adult rats. *Learning & memory*, 16, 147–154.
- 1255 Johnston, S. T., Shtrahman, M., Parylak, S., Gonçalves, J. T., and Gage, F. H.
1256 (2016). Paradox of pattern separation and adult neurogenesis: A dual role
1257 for new neurons balancing memory resolution and robustness. *Neurobiology of*
1258 *learning and memory*, 129, 60–68.
- 1259 Kee, N., Teixeira, C. M., Wang, A. H., and Frankland, P. W. (2007). Preferential
1260 incorporation of adult-generated granule cells into spatial memory networks in
1261 the dentate gyrus. *Nature neuroscience*, 10, 355–362.
- 1262 Khazipov, R., Khalilov, I., Tyzio, R., Morozova, E., Ben-Ari, Y., and Holmes,
1263 G. L. (2004). Developmental changes in GABAergic actions and seizure suscep-
1264 tibility in the rat hippocampus. *European Journal of Neuroscience*, 19, 590–600.
- 1265 Klausberger, T. and Somogyi, P. (2008). Neuronal diversity and temporal dy-
1266 namics: the unity of hippocampal circuit operations. *Science*, 321, 53–57.
- 1267 Kohonen, T. (1989). *Self-organization and associative memory*. (Springer-Verlag),
1268 3rd edn.
- 1269 LeCun, Y., Bottou, L., Bengio, Y., and Haffner, P. (1998). Gradient-based learn-
1270 ing applied to document recognition. *Proceedings of the IEEE*, 86, 2278–2324.
- 1271 Leonzino, M., Busnelli, M., Antonucci, F., Verderio, C., Mazzanti, M., and Chini,
1272 B. (2016). The timing of the excitatory-to-inhibitory GABA switch is regulated
1273 by the oxytocin receptor via KCC2. *Cell reports*, 15, 96–103.
- 1274 Li, L., Sultan, S., Heigele, S., Schmidt-Salzman, C., Toni, N., and Bischofberger,
1275 J. (2017). Silent synapses generate sparse and orthogonal action potential firing
1276 in adult-born hippocampal granule cells. *Elife*, 6, e23612.
- 1277 Li, Y., Stam, F. J., Aimone, J. B., Goulding, M., Callaway, E. M., and Gage,
1278 F. H. (2013). Molecular layer perforant path-associated cells contribute to feed-
1279 forward inhibition in the adult dentate gyrus. *Proceedings of the National*
1280 *Academy of Sciences*, 110, 9106–9111.

- 1281 Mardia, K. V. and Jupp, P. E. (2009). Directional statistics, vol. 494. (John
1282 Wiley & Sons).
- 1283 Marín-Burgin, A., Mongiat, L. A., Pardi, M. B., and Schinder, A. F. (2012).
1284 Unique processing during a period of high excitation/inhibition balance in
1285 adult-born neurons. *Science*, 335, 1238–1242.
- 1286 Marr, D. (1969). A theory of cerebellar cortex. *J. Physiology*, 202, 437–470.
- 1287 Marr, D. (1971). Simple memory: a theory for archicortex. *Philosophical Trans-*
1288 *actions of the Royal Society of London*, 262, 23–81.
- 1289 McHugh, T. J., Jones, M. W., Quinn, J. J., Balthasar, N., Coppari, R., Elmquist,
1290 J. K., Lowell, B. B., Fanselow, M. S., Wilson, M. A., and Tonegawa, S. (2007).
1291 Dentate gyrus NMDA receptors mediate rapid pattern separation in the hip-
1292 pocampal network. *Science*, 317, 94–99.
- 1293 Miller, K. D. and Fumarola, F. (2012). Mathematical equivalence of two common
1294 forms of firing rate models of neural networks. *Neural computation*, 24, 25–31.
- 1295 Owens, D. F. and Kriegstein, A. R. (2002). Is there more to GABA than synaptic
1296 inhibition? *Nature Reviews Neuroscience*, 3, 715–727.
- 1297 Pathak, H. R., Weissinger, F., Terunuma, M., Carlson, G. C., Hsu, F.-C., Moss,
1298 S. J., and Coulter, D. A. (2007). Disrupted dentate granule cell chloride reg-
1299 ulation enhances synaptic excitability during development of temporal lobe
1300 epilepsy. *Journal of Neuroscience*, 27, 14012–14022.
- 1301 Pfister, J.-P. and Gerstner, W. (2006). Triplets of spikes in a model of spike
1302 timing-dependent plasticity. *Journal of Neuroscience*, 26, 9673–9682.
- 1303 Rolls, E. T. and Treves, A. (1998). *Neural networks and brain function*, vol. 572.
1304 (Oxford university press Oxford).
- 1305 Rumelhart, D. E. and Zipser, D. (1985). Feature discovery by competitive learn-
1306 ing. *Cognitive science*, 9, 75–112.
- 1307 Sahay, A., Scobie, K. N., Hill, A. S., O’Carroll, C. M., Kheirbek, M. A., Burghardt,
1308 N. S., Fenton, A. A., Dranovsky, A., and Hen, R. (2011a). Increasing adult
1309 hippocampal neurogenesis is sufficient to improve pattern separation. *Nature*,
1310 472, 466–470.
- 1311 Sahay, A., Wilson, D. A., and Hen, R. (2011b). Pattern separation: a common
1312 function for new neurons in hippocampus and olfactory bulb. *Neuron*, 70, 582–
1313 588.

- 1314 Schmidt-Hieber, C., Jonas, P., and Bischofberger, J. (2004). Enhanced synaptic
1315 plasticity in newly generated granule cells of the adult hippocampus. *Nature*,
1316 429, 184–187.
- 1317 Senzai, Y. and Buzsáki, G. (2017). Physiological properties and behavioral corre-
1318 lates of hippocampal granule cells and mossy cells. *Neuron*, 93, 691–704.
- 1319 Sjöström, P., Turrigiano, G., and Nelson, S. (2001). Rate, timing, and coopera-
1320 tivity jointly determine cortical synaptic plasticity. *Neuron*, 32, 1149–1164.
- 1321 Somogyi, P. and Klausberger, T. (2005). Defined types of cortical interneurone
1322 structure space and spike timing in the hippocampus. *The Journal of physiology*,
1323 562, 9–26.
- 1324 Stefanelli, T., Bertollini, C., Lüscher, C., Muller, D., and Mendez, P. (2016).
1325 Hippocampal somatostatin interneurons control the size of neuronal memory
1326 ensembles. *Neuron*, 89, 1074–1085.
- 1327 Tashiro, A., Makino, H., and Gage, F. H. (2007). Experience-specific functional
1328 modification of the dentate gyrus through adult neurogenesis: a critical period
1329 during an immature stage. *Journal of Neuroscience*, 27, 3252–3259.
- 1330 Tashiro, A., Sandler, V. M., Toni, N., Zhao, C., and Gage, F. H. (2006). NMDA-
1331 receptor-mediated, cell-specific integration of new neurons in adult dentate
1332 gyrus. *Nature*, 442, 929–933.
- 1333 Temprana, S. G., Mongiat, L. A., Yang, S. M., Trincherro, M. F., Alvarez, D. D.,
1334 Kropff, E., Giacomini, D., Beltramone, N., Lanuza, G. M., and Schinder, A. F.
1335 (2015). Delayed coupling to feedback inhibition during a critical period for the
1336 integration of adult-born granule cells. *Neuron*, 85, 116–130.
- 1337 Tyzio, R., Holmes, G. L., Ben-Ari, Y., and Khazipov, R. (2007). Timing of the de-
1338 velopmental switch in GABA_A mediated signaling from excitation to inhibition
1339 in CA3 rat hippocampus using gramicidin perforated patch and extracellular
1340 recordings. *Epilepsia*, 48, 96–105.
- 1341 Van Praag, H., Kempermann, G., and Gage, F. H. (1999). Running increases
1342 cell proliferation and neurogenesis in the adult mouse dentate gyrus. *Nature*
1343 *neuroscience*, 2, 266–270.
- 1344 Vivar, C., Potter, M. C., Choi, J., Lee, J.-y., Stringer, T. P., Callaway, E. M.,
1345 Gage, F. H., Suh, H., and Van Praag, H. (2012). Monosynaptic inputs to new
1346 neurons in the dentate gyrus. *Nature Communications*, 3, 1107.
- 1347 Wang, D. D. and Kriegstein, A. R. (2010). Blocking early GABA depolariza-
1348 tion with bumetanide results in permanent alterations in cortical circuits and
1349 sensorimotor gating deficits. *Cerebral cortex*, 21, 574–587.

- 1350 Wang, Y., Chik, D. T. W., and Wang, Z. D. (2000). Coherence resonance
1351 and noise-induced synchronization in globally coupled Hodgkin-Huxley neu-
1352 rons. *Phys. Rev. E*, 61, 740.
- 1353 Weisz, V. I. and Argibay, P. F. (2009). A putative role for neurogenesis in neu-
1354 rocomputational terms: Inferences from a hippocampal model. *Cognition*, 112,
1355 229–240.
- 1356 Weisz, V. I. and Argibay, P. F. (2012). Neurogenesis interferes with the retrieval
1357 of remote memories: Forgetting in neurocomputational terms. *Cognition*, 125,
1358 13–25.
- 1359 Wiskott, L., Rasch, M. J., and Kempermann, G. (2006). A functional hypothesis
1360 for adult hippocampal neurogenesis: avoidance of catastrophic interference in
1361 the dentate gyrus. *Hippocampus*, 16, 329–343.
- 1362 Woods, N. I., Stefanini, F., Apodaca-Montano, D. L., Tan, I. M., Biane, J. S., and
1363 Kheirbek, M. A. (2020). The dentate gyrus classifies cortical representations of
1364 learned stimuli. *Neuron*, 107.
- 1365 Yeckel, M. F. and Berger, T. W. (1990). Feedforward excitation of the hip-
1366 pocampus by afferents from the entorhinal cortex: redefinition of the role of
1367 the trisynaptic pathway. *Proceedings of the National Academy of Sciences*, 87,
1368 5832–5836.
- 1369 Yuan, M., Meyer, T., Benkowitz, C., Savanthrapadian, S., Ansel-Bollepalli, L.,
1370 Foggetti, A., Wulff, P., Alcami, P., Elgueta, C., and Bartos, M. (2017).
1371 Somatostatin-positive interneurons in the dentate gyrus of mice provide local-
1372 and long-range septal synaptic inhibition. *eLife*, 6, e21105.
- 1373 Zenke, F. and Gerstner, W. (2017). Hebbian plasticity requires compensatory pro-
1374 cesses on multiple timescales. *Philosophical Transactions of the Royal Society*
1375 *B: Biological Sciences*, 372, 1–17.
- 1376 Zhao, C., Teng, E. M., Summers, R. G., Ming, G.-l., and Gage, F. H. (2006).
1377 Distinct morphological stages of dentate granule neuron maturation in the adult
1378 mouse hippocampus. *Journal of Neuroscience*, 26, 3–11.

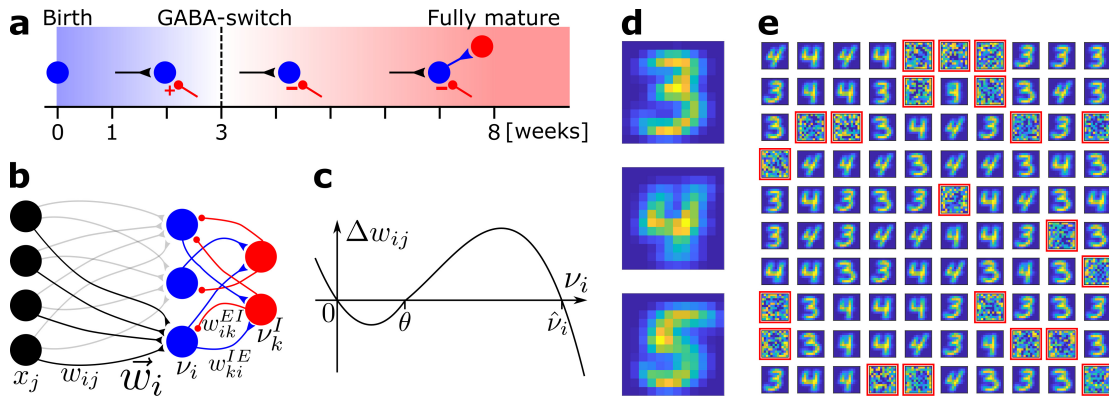


Figure 1: Network model and pretraining. (a) Integration of an adult-born DGC (blue) as a function of time: GABAergic synaptic input (red) switches from excitatory (+) to inhibitory (-); strong connections to interneurons develop only later; glutamatergic synaptic input (black), interneuron (red). (b) Network structure. EC neurons (black, rate x_j) are fully connected with weights w_{ij} to DGCs (blue, rate ν_i). The feedforward weight vector \vec{w}_i onto neuron i is depicted in black. DGCs and interneurons (red, rate ν_k^I) are mutually connected with probability p_{IE} and p_{EI} and weights w_{ki}^{IE} and w_{ik}^{EI} , respectively. Connections with a triangular (round) end are glutamatergic (GABAergic). (c) Given presynaptic activity $x_j > 0$, the weight update Δw_{ij} is shown as a function of the firing rate ν_i of the postsynaptic DGC with LTD for $\nu_i < \theta$ and LTP for $\theta < \nu_i < \hat{\nu}_i$. (d) Center of mass for three ensembles of patterns from the MNIST data set, visualized as 12x12 pixel patterns. The two-dimensional arrangements and colors are for visualization only. (e) 100 receptive fields, each defined as the set of feedforward weights, are represented in a 2-dimensional organization. After pretraining with patterns from MNIST digits 3 and 4, 79 DGCs have receptive fields corresponding to threes and fours of different writing styles, while 21 remain unselective (highlighted by red frames).

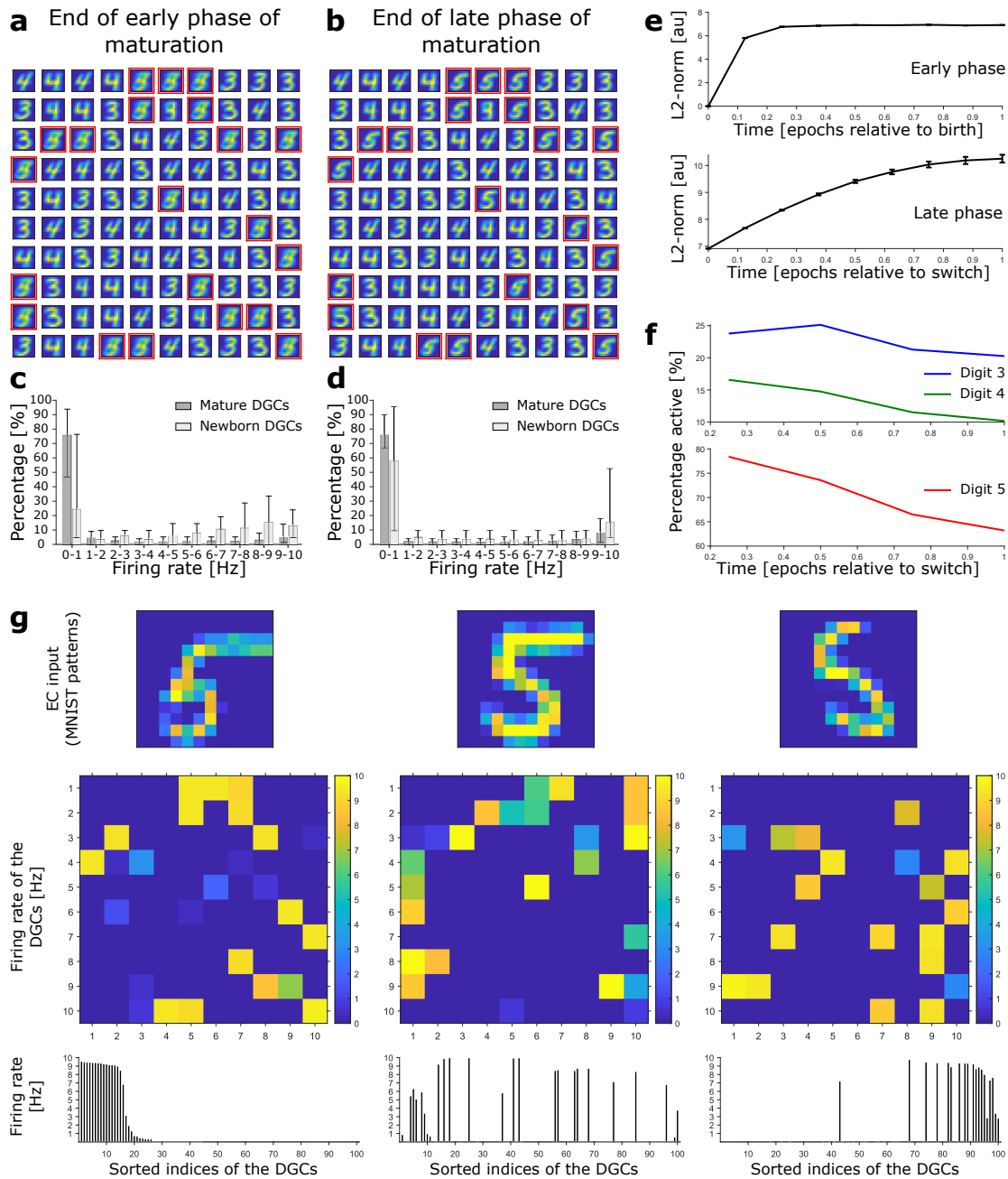


Figure 2: Newborn DGCs become selective for novel patterns during maturation.

1379 **Figure 2: Newborn DGCs become selective for novel patterns during**
1380 **maturation.** (a) Unselective neurons are replaced by newborn DGCs, which
1381 learn their feedforward weights while patterns from digits 3, 4, and 5 are presented.
1382 At the end of the early phase of maturation, the receptive fields of all newborn
1383 DGCs (red frames) show mixed selectivity. (b) At the end of the late phase
1384 of maturation, newborn DGCs are selective for patterns from the novel digit
1385 5, with different writing styles. (c,d) Distribution of the percentage of model
1386 DGCs (mean with 10th and 90th percentiles) in each firing rate bin at the end
1387 of the early (c) and late (d) phase of maturation. Statistics calculated across
1388 MNIST patterns ('3's, '4's, '5's). Percentages are per subpopulation (mature and
1389 newborn). Note that neurons with firing rate $< 1\text{Hz}$ for one pattern may fire at
1390 medium or high rate for another pattern. (e) The L2-norm of the feedforward
1391 weight vector onto newborn DGCs (mean \pm SEM) increases as a function of
1392 maturation indicating growth of synapses and receptive field strength. Horizontal
1393 axis: time=1 indicates end of early (top) or late phase (bottom). (f) Percentage
1394 of newborn DGCs activated (firing rate $> 1\text{Hz}$) by a stimulus averaged over all
1395 test patterns as a function of maturation. (g) At the end of the late phase of
1396 maturation, three different patterns of digit 5 applied to EC neurons (top) cause
1397 different firing rate patterns of the 100 DGCs arranged in a matrix of 10-by-10
1398 cells (middle). DGCs with a receptive field (see Fig. 2b) similar to a presented EC
1399 activation pattern respond more strongly than the others. Bottom: Firing rates of
1400 the DGCs with indices sorted from highest to lowest firing rate in response to the
1401 first pattern. All 3 patterns shown come from the testing set, and are correctly
1402 classified using our readout network.

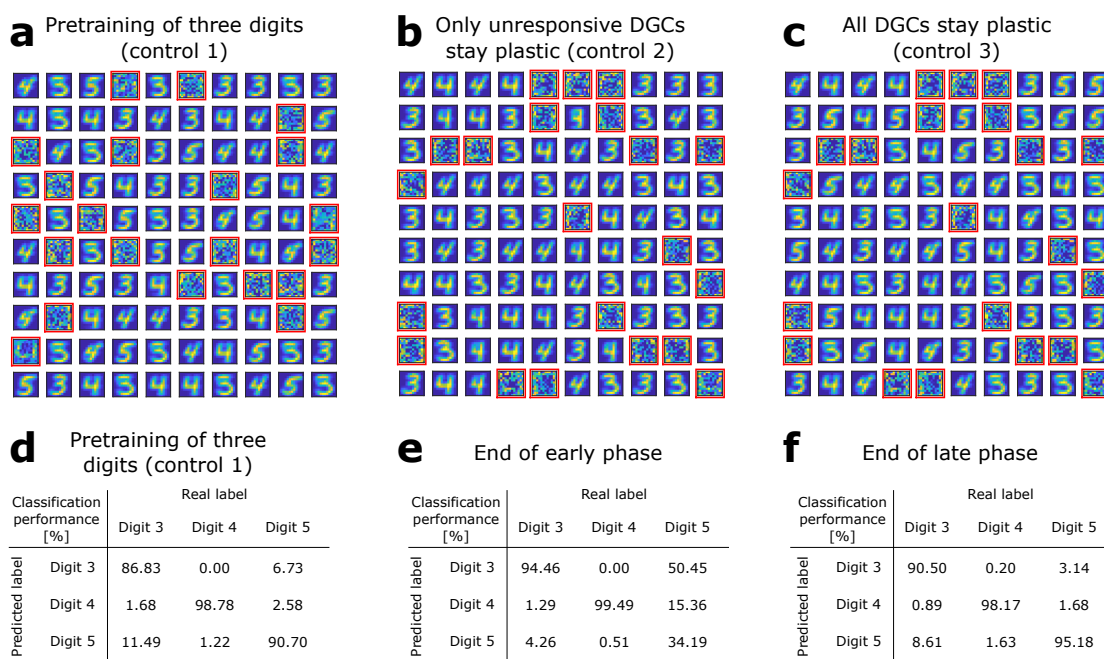


Figure 3: The GABA-switch guides learning of novel representations.

(a) Pretraining on digits 3, 4 and 5 simultaneously without neurogenesis (control 1). Patterns from digits 3, 4 and 5 are presented to the network while all DGCs learn their feedforward weights. After pretraining, 79 DGCs have receptive fields corresponding to the three learned digits, while 21 remain unselective (as in Fig. 1e). (b) Sequential training without neurogenesis (control 2). After pretraining as in Fig. 1e, the unresponsive neurons stay plastic, but they fail to become selective for digit 5 when patterns from digits 3, 4, and 5 are presented in random order. (c) Sequential training without neurogenesis but all DGCs stay plastic (control 3). Some of the DGCs previously responding to patterns from digits 3 or 4 become selective for digit 5. (d-f) Confusion matrices. Classification performance in percent (using a linear classifier as readout network) for control 1 (d) and for the standard model at the end of the early (e) and late (f) phase; cf. Fig. 2a,b.

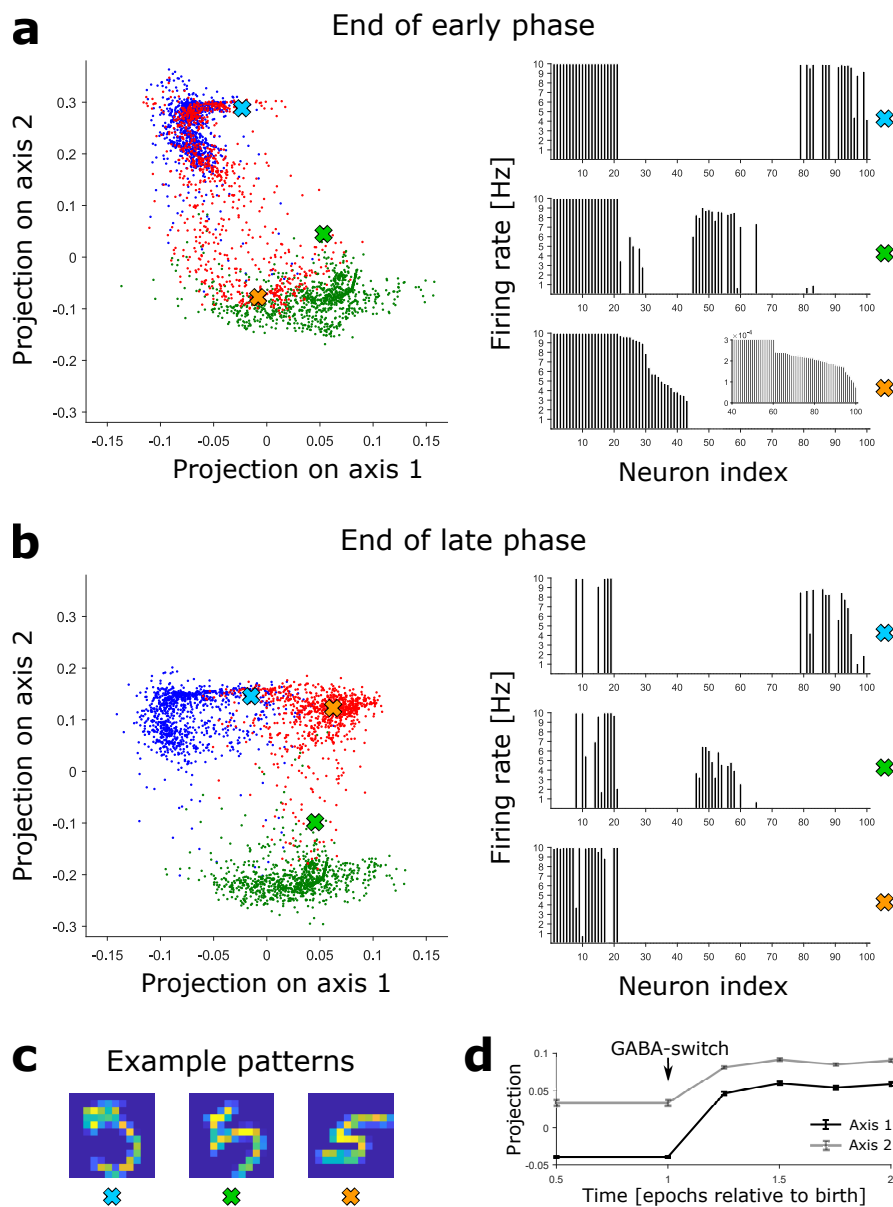


Figure 4: Novel patterns expand the representation into a previously empty subspace. (a) Left: The DGC activity responses at the end of the early phase of maturation of newborn DGCs are projected on discriminatory axes. Each point corresponds to the representation of one input pattern. Color indicates digit 3 (blue), 4 (green), and 5 (red). Right: Firing rate profiles of three example patterns (highlighted by crosses on the left) are sorted from high to low for the pattern represented by the orange cross (inset: zoom of firing rates of DGCs with low activity). (b) Same as a, but at the end of the late phase of maturation of newborn DGCs. Note that the red dots around the orange cross have moved into a different subspace. (c) Example patterns of digit 5 corresponding to the symbols in a and b. All three are accurately classified by our readout network. (d) Evolution of the mean (\pm SEM) of the projection of the activity upon presentation of all test patterns of digit 5.

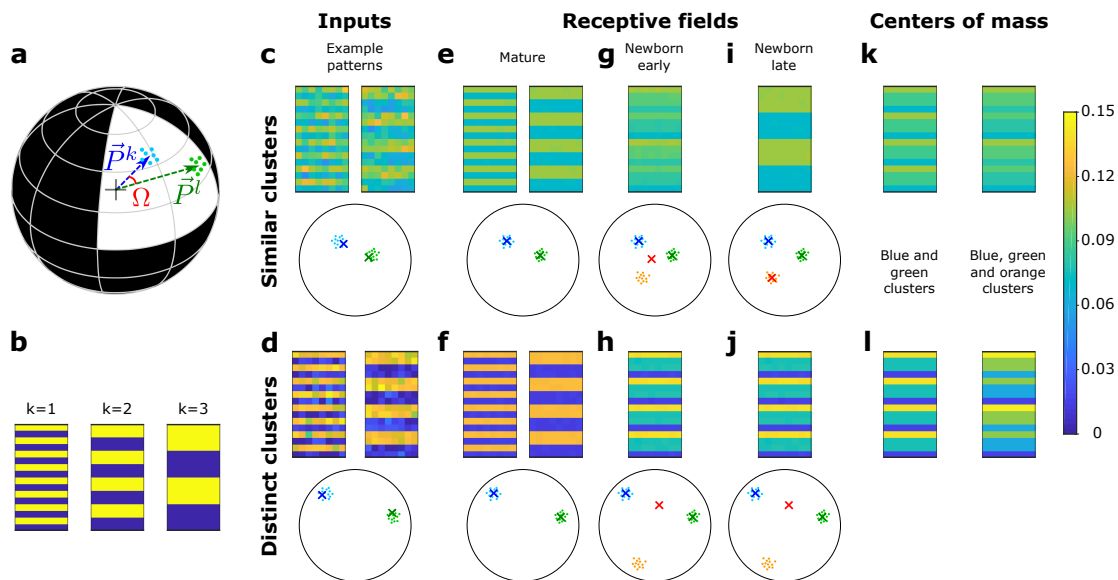


Figure 5: A newborn DGC becomes selective for similar but not distinct novel stimuli.

1403 **Figure 5: A newborn DGC becomes selective for similar but not distinct**
1404 **novel stimuli.** (a) Center of mass of clusters k and l of an artificial data set (\vec{P}_k
1405 and \vec{P}_l , respectively, separated by angle Ω) are represented by arrows that point
1406 to the surface of a hypersphere. Dots represent individual patterns. (b) Center of
1407 mass of three clusters of the artificial data set, visualized as 16x8 pixel patterns.
1408 The two-dimensional arrangements and colors are for visualization only. (c,d)
1409 Example input patterns (activity of 16x8 input neurons) from clusters 1 and 2
1410 for similar clusters (c, $s = 0.8$), and distinct clusters (d, $s = 0.2$). Below: dots
1411 correspond to patterns, crosses indicate the input patterns shown (schematic).
1412 (e,f) After pretraining with patterns from two clusters, the receptive fields (set of
1413 synaptic weights onto neurons 1 and 2) exhibit the center of mass of each cluster
1414 of input patterns (blue and green crosses). (g,h) Novel stimuli from cluster 3
1415 (orange dots) are added. If the clusters are similar, the receptive field of the
1416 newborn DGC (red cross) moves towards the center of mass of the three clusters
1417 during its early phase of maturation (g), and if the clusters are distinct towards
1418 the center of mass of the two pretrained clusters (h). (i,j) Receptive field after the
1419 late phase of maturation for the case of similar (i) or distinct (j) clusters. (k,l) For
1420 comparison, the center of mass of all patterns of the blue and green clusters (left
1421 column) and of the blue, green and orange clusters (right column) for the case of
1422 similar (k) or distinct (l) clusters. Color scale: input firing rate \vec{x} or weight \vec{w}_i
1423 normalized to $\|\vec{w}_i\| = 1 = \|\vec{x}\|$.

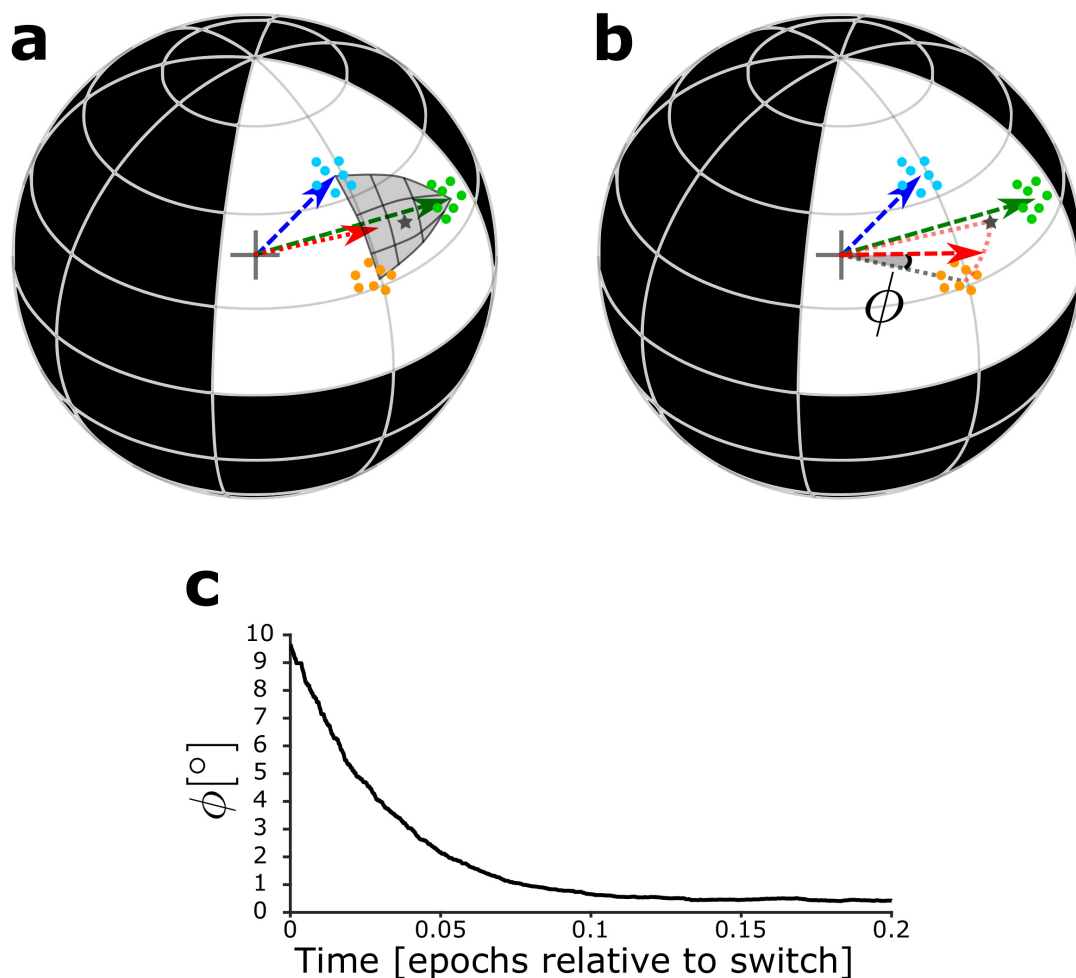


Figure 6: Maturation dynamics for similar patterns. (a) Schematics of the unit hypersphere with three clusters of patterns (colored dots) and three scaled feedforward weight vectors (colored arrows). After pretraining, the blue and green weight vectors point to the center of mass of the corresponding clusters. Patterns from the novel cluster (orange points) are presented only later to the network. During the early phase of maturation, the newborn DGC grows its vector of feedforward weights (red arrow) in the direction of the subspace of patterns which indirectly activate the newborn cell (dark grey star: center of mass of the presented patterns, located below the part of the sphere surface highlighted in grey). (b) During the late phase of maturation, the red vector turns towards the novel cluster. Angle ϕ between the center of mass of the novel cluster and the feedforward weight vector onto the newborn cell. (c) The angle ϕ decreases in the late phase of maturation of the newborn DGC if the novel cluster is similar to the previously stored clusters. Its final average value of $\phi \approx 0.4^\circ$ is caused by the jitter of the weight vector around the center of mass of the novel cluster.

Table 1: Parameters for the simulations

	Biologically-plausible network		Simplified network	
Network	$N_{EC} = 144$ $N_I = 25$	$N_{DGC} = 100$	$N_{EC} = 128$	$N_{DGC} = 3$
Connectivity	$w_{IE} = 1$ $p_{IE} = 0.9$	$w_{EI} = -\frac{1}{p_{EI} * N_I}$ $p_{EI} = 0.9$	$w_{rec} = -1.2$	
Dynamics	$\tau_m = 20$ ms $L = 0.5$	$\tau_{inh} = 2$ ms $p^* = 0.1$	$\tau_m = 20$ ms	
Plasticity	$\alpha_0 = 0.05$ $\gamma_0 = 10$ $\nu_0 = 0.2$	$\beta = 1$ $\theta = 0.15$ $\gamma = 9.85$	$\alpha_0 = 0.03$ $\gamma_0 = 1.65$ $\gamma = 1.5$	$\beta = 1$ $\theta = 0.15$
Numerical simulations	$\Delta t = 0.1$ ms $\eta_b = 0.01$	$\eta = 0.01$	$\Delta t = 1$ ms	$\eta = 0.01$